Robotica (2002) volume 20, pp. 33–48. © 2002 Cambridge University Press
DOI: 10.1017/S0263574701003526 Printed in the United Kingdom

Note on the relative degree of a flexible manipulator and implications to inverse dynamics for tracking control

G.L. Wang* and H. Unbehauen

Control Engineering Laboratory, Faculty of Electrical Engineeering, Ruhr-University Bochum, 44780 Bochum (Germany)

(Received in Final Form: April 20, 2001)

SUMMARY

This paper rechecks the relative degree of the end-point tracking control system of a flexible manipulator. New added insights into the ill-defined behavior of the relative degree are presented by constructing a perturbed truncation model. The implications for the inverse dynamics motivate us to reformulate the inverse dynamics based on the perturbed truncation model in the extreme case of truncating all of the flexible modes. New potential advantages arising from this novel formulation are investigated for the inverse dynamics control design as well.

KEYWORDS: Inverse dynamics; Flexible manipulator, Tracking control; Truncation model.

1. INTRODUCTION

In the past decade, the end-effector tracking control of flexible manipulators has been well studied. The non-minimum phase zeros arising from the noncolocated actuator/sensor structure have a negative effect on a feedback-based regulator's ability to reduce tracking errors[1] and some fundamental limitation on transient tracking performance exists. The inverse dynamic control approach can overcome the transient error phenomenon; thus it is preferred to the feedback regulation for exact tip output trajectory tracking. The pioneering work on the inverse dynamics of flexible manipulators can be found in Bayo et al.,[2] in which the frequency-domain approach was developed. The time-domain formulation for linear systems was presented in Know and Book[3] and successful experimental studies were conducted by Paden et al.[4] and De Luca et al.[5] A major advance in the formalized treatment was made by introducing the framework of a stable inversion based approach in Devasia et al.[6] and Chen and Paden;[7] a further extension of this idea was made by Hunt et al.,[8,9] so that this approach became applicable to aircraft guidance control systems.[10,11] The stable inversion based approach differs from the earlier output tracking approaches in that (i) the reference trajectories to be tracked are the tracking-task-oriented time-functions rather than the outputs of some exosystems like in the former regulation approach;[12] (ii) the noncausal bounded solutions of the unstable zero dynamics are sought for nonminimum phase systems, which is in contrast to the causal inversion approach,[13] where unstable zero dynamics lead to unbounded solutions; (iii) there is no special initial condition settlement as is done in Di Benedetto and Lucibello[14] because the preactuation establishes the initial conditions implicitly when nonminimum phase systems are considered.

The key to the stable inversion based approach is that the relative degree of a system is well-defined to ensure the recovery of the input from the output. However, as the net displacement of the end-effector is used as the output variable, the input-output relative degree of a flexible manipulator is ill-defined,[15,16] and the inverse dynamics becomes ill-conditioned. This can lead to actuator high-frequency saturation that deteriorates the tracking performance.[17] To prevent the occurrence of actuator high-frequency saturation, one possibility is to select smooth trajectories to be tracked; this can be done carefully by trajectory planning.[18–21] An alternative approach is to redefine the output variable so that the relative degree is well-defined. Wang and Vidyasagar[16] introduced the reflected tip output, a rigid body motion minus elastic deformation, to yield a passivity transfer function with the well-defined relative degree being two. Other well-behaved transfer functions were studied in Barbieri.[22] De Luca et al.[23] showed that taking some suitable points along a link as the output, the passivity property could be guaranteed. The extreme case is that the joint-space based trajectory tracking system always preserves the well-conditioned inversion.[24] For large payloads, the modified output, the so-called μ-tip rate, leads to an approximate minimum phase dynamics.[25] Although output-variable redefining can maintain preferable properties for the control design, its direct application is limited to cases where the tip position is not crucial, except near the end of a maneuver.

The practical implementation of the inverse dynamics control requires a finite dimensional approximation to the original infinite dimensional model of flexible manipulators. For that purpose it is a common practice to remove the modes which correspond to frequencies that lie out of the bandwidth of sensors and actuators and to keep the modes which directly contribute to the low-frequency dynamics. In this way, the approximation to the tip output excludes the contributions from the truncated high-order modes. One known drawback of this direct truncation approach is the poor prediction of the tip position zeros of a single-link flexible manipulator.[26] The inverse dynamics control design

* The permanent address is: Department of Computer Science, Shantou University, 515063 Shantou, P.R. China. Currently he is a visiting scientist as an Alexander von Humboldt Research Fellow with Prof. Dr.-Ing Heinz Unbehauen.
Email:glwang@esr.ruhr-uni-bochum.de

is heavily sensitive to the tip position zeros because the poles of internal dynamics are exactly the same as these zeros. Then the question arises: Can the finite dimensional approximation via this direct truncation predict the ill-defined behavior of the relative degree well? This problem motivates this work to recheck the relative degree of the end-point tracking control system of a flexible manipulator. The main contribution of this paper is to provide some new added insights into the ill-defined behavior of the relative degree via constructing a perturbed truncation model, and to reformulate the inverse dynamics control design in a novel way.

To exhibit the ill-defined behavior of the relative degree well, the contributions from all of the truncated high-order modes should be accounted for in the finite dimensional approximation. In this paper, we do this by retaining all of the flexible modes in the modal expansion of the tip output. To achieve the finite dimensional approximation, we truncate the fast transients of the high-order flexible modes, but embed their quasi-steady-states as perturbations into the tip output to form the perturbed truncation model. The idea of constructing this perturbed truncation model integrates the model approximation approach based on the singular perturbation method[27] and the standard modal truncation method. The related ideas of using the singular perturbation method were reported in Siciliano and Book[28] and Vandegrift et al.,[29] however, mainly for the purpose of the joint-space based tracking control[23,24] rather than the tip tracking control. With this perturbed truncation model, new added insights into the ill-defined behavior of the relative degree are presented. In addition, based on the perturbed truncation model, the reformulation of the inverse dynamics control design is investigated. In doing this, we truncate the fast transients of the flexible dynamics and keep only that of the rigid dynamics. There are two potential advantages arising from this novel formulation of the inverse dynamics control design. First, the inverse dynamics control design based on the perturbed truncation model can be used to track not much smoothing trajectories, especially since it is unnecessarily twice differentiable, thus it holds great promise to a much wider range of practical applications. Indeed, this advantage leads to flexibility. Second, this formulation leads to nearly linear and time-invariant internal dynamics with a relatively lower order for multi-link flexible manipulators. Its simplicity makes the inverse dynamics control design practically useful.

This paper is organized as follows: In the next section, the motivated studies are presented in the context of a single-link flexible manipulator for clarity. In Section 3 we extend the main results to multi-link flexible manipulators. At the end of this paper, numerical simulations are presented to illustrate the methods proposed.

2. MOTIVATED STUDY ON SINGLE-LINK FLEXIBLE MANIPULATOR

2.1. Modal model

Consider a typical planar single-link flexible arm depicted in Figure 1, where the inertia frame is denoted by *OXY* and the rotating frame by *Oxy*. The tip of the link is attached to a payload that is modeled as a concentrated mass M_t and the other end to a hub of inertia J_h connected to the actuator that is located at the point *O* and supplies the torque τ. The link is assumed to be a uniform slender beam that satisfies the assumption of Euler-Bernoulli beam theory. Let l be the length of the link, ρ the mass per length, E the Young modulus, I the moment of inertia. The net displacement of the flexible link is expressed approximately by

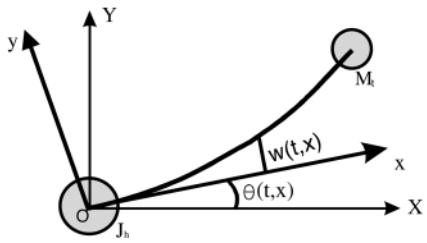

Fig. 1. Schematic diagram of a planar single-link flexible arm.

$$z(t, x) = x\theta(t) + w(t, x), \tag{1}$$

where $\theta(t)$ is the rotation angle of the hub, and $w(t, x)$ is the deflection in the rotating frame *Oxy*. The modal expansion of $z(t, x)$ is $z(t, x) = \sum_{n=0}^{\infty} \phi_n(x) q_n(t)$, where $q_n(t)$ is the modal coordinate of the nth unconstrained mode function $\phi_n(x)$. For each n, q_n satisfies the equation of

$$\ddot{q}_n + \omega_n^2 q_n = \psi_n \tau, \tag{2}$$

where ω_n is the natural frequency of the nth mode and $\psi_n = \mathrm{d}\phi_n/\mathrm{d}x(0)$ (see Appendix A). For the purpose of the tip trajectory tracking control, define the tip net displacement as the output

$$y =: z(t, l) = \sum_{n=0}^{\infty} q_n \varphi_n, \tag{3}$$

where $\varphi_n = \phi_n(l)$. The endpoint sensor and root actuator locations trivially guarantee that $\psi_n \neq 0$, $\varphi_n \neq 0$, $n = 1, 2, \ldots$.

2.2 Direct truncation of modal model

Before the inverse dynamics control design can be developed, a finite dimensional approximation to the above infinite dimensional model is necessary. For this purpose it is common practice to truncate the high-frequency modes which lie out of the bandwidth of interest and to retain the rest modes which directly contribute to the low-frequency dynamics of the system. Note that q_0 corresponds to the rigid mode and $\omega_0 = 0$. Define the vector of the first Nth flexible coordinates as $\boldsymbol{q}_f = [q_1 \ldots q_N]^T$. The direct truncation of the first Nth flexible mode means that we retain the first Nth flexible modes and truncate the rest high-order modes. This procedure yields

$$\begin{bmatrix} \ddot{q}_0 \\ \ddot{\boldsymbol{q}}_f \end{bmatrix} = \begin{bmatrix} 0 & \mathbf{0} \\ \mathbf{0}^T & -\boldsymbol{\Omega} \end{bmatrix} \begin{bmatrix} q_0 \\ \boldsymbol{q}_f \end{bmatrix} + \begin{bmatrix} \psi_0 \\ \boldsymbol{\psi}_f \end{bmatrix} \tau, \tag{4}$$

where $\boldsymbol{\Omega} = \mathrm{diag}(\omega_1^2 \omega_2^2 \ldots \omega_N^2)$ and $\boldsymbol{\psi}_f = [\psi_1\ \psi_2 \ldots \psi_N]^T$. Here $'\mathbf{0}'$ are appropriate sized submatrices consisting merely of

https://doi.org/10.1017/S0263574701003526 Published online by Cambridge University Press

zero elements. This notation will be used throughout this paper. The resulting approximation to the output is

$$\tilde{y} = \varphi_0 q_0 + \boldsymbol{\varphi}_f^T \boldsymbol{q}_f, \tag{5}$$

where $\boldsymbol{\varphi}_f^T = [\varphi_1\ \varphi_2\ \ldots\ \varphi_N]$.

To check the relative degree of the above finite dimensional approximation, the output $\tilde{y}(t)$ needs to be differentiated successively until the input $\tau(t)$ appears in the derivative expression. This leads to

$$\ddot{\tilde{y}} = -\boldsymbol{\varphi}_f^T \boldsymbol{\Omega} \boldsymbol{q}_f + \tilde{\epsilon}_N \tau, \tag{6}$$

where $\tilde{\epsilon}_N = \varphi_0 \psi_0 + \boldsymbol{\varphi}_f^T \boldsymbol{\psi}_f$. It is easy to see that the relative degree of the above finite dimensional approximation is equal to two. According to the asymptotical analysis of the unconstrained modes (see Appendix A), we have that $\tilde{\epsilon}_N = (-1)^N |O((N+1)^{-2})|$. Reducing singularity effects requires the reduction of the index N. The extreme case of $N=0$ is to recover the rigid system. However, excluding the modes which lie within the bandwidth of the actuator can lead to instability. Thus there exists a limitation on the reduction of the truncation index N. Actually, this limitation attributes to the poor prediction of the ill-defined behavior of the relative degree via the direct truncation. This point will be explained later.

For a given reference tip trajectory y_d, the procedure for solving the inverse dynamics is as follows. With $\ddot{y}_d$ instead of $\ddot{\tilde{y}}$ inverting (6) gives

$$\tilde{\tau}_d = \tilde{\epsilon}_N^{-1} (\ddot{y}_d + \boldsymbol{\varphi}_f^T \boldsymbol{\Omega} \boldsymbol{q}_f). \tag{7}$$

Substituting this into (4) yields for the flexible modes

$$\ddot{\boldsymbol{q}}_f = (-\boldsymbol{\Omega} + \tilde{\epsilon}_N^{-1} \boldsymbol{\psi}_f \boldsymbol{\varphi}_f^T \boldsymbol{\Omega}) \boldsymbol{q}_f + \tilde{\epsilon}_N^{-1} \boldsymbol{\psi}_f \ddot{y}_d, \tag{8}$$

and for the rigid mode

$$\ddot{q}_0 = \psi_0 \boldsymbol{\varphi}_f^T \boldsymbol{\Omega} \boldsymbol{q}_f + \tilde{\epsilon}_N^{-1} \psi_0 \ddot{y}_d. \tag{9}$$

(8) describes the so-called internal dynamics. To distinguish from the solutions of (4), $\tilde{\boldsymbol{q}}_f$ and $\tilde{q}_0$ denote the solutions of (8) and (9), respectively. Once the stable solution of the internal dynamics (8), $\tilde{\boldsymbol{q}}_f(t)$, is found, the nominal torque $\tilde{\tau}_d(t)$ is followed from (7), and the desired trajectory of the rigid mode coordinate, $\tilde{q}_0$, can be obtained by (9). It should be noted that the internal dynamics (8) has no poles on the imaginary axis but has poles in the half right plane; thus, the bounded solutions of the inverse dynamics must be noncausal. These noncausal solutions can be solved in the time domain[3] or in the frequency domain.[30]

2.3 Perturbed truncation of modal model

To show the ill-defined behavior of the relative degree well, the contributions from all of the truncated high-order modes should be accounted for in the finite dimensional approximation. We do this by retaining all of the flexible modes in the modal expansion of the tip output. To achieve the finite dimensional approximation, we truncate the fast transients of the high-order flexible modes but embed their quasi-steady-states as perturbations into the tip output to form the perturbed truncation model. This idea integrates the model approximation approach based on the singular perturbation method[27] and the standard modal truncation method.

Note that $\omega_n^2 = O(n^4)$ (see Appendix A). This reveals the multi-time-scale characteristics in the modal model. Based on the truncation index N, we split the flexible modes into two groups: slow modes $\{q_n\}_{n=1}^{N}$ and fast modes $\{q_n\}_{n=N+1}^{\infty}$. According to the singular perturbation analysis,[27] for the fast modes, we can represent (2) as the singular perturbation form of

$$\mu_n^2 \ddot{\xi}_n + \xi_n = \psi_n \tau, \tag{10}$$

where $\mu_n = \omega_n^{-1}$ is the time scale or the singular perturbation parameter, and $q_n = \mu_n^2 \xi_n$. Making the singular parameter $\mu_n = 0$ in (10) yields the following degenerated form as

$$\bar{\xi}_n = \psi_n \tau,$$

which is the first-order approximation to (10) with respect to the perturbation parameter. Thus for each $n > N$, q_n can be approximated by

$$q_n \approx \bar{q}_n = \omega_n^{-2} \psi_n \tau. \tag{11}$$

For all of $n > N$, substituting (11) into the output (3) gives the perturbed approximation to the output as

$$\bar{y} = \tilde{y} + \bar{\epsilon}_N \tau = \varphi_0 q_0 + \boldsymbol{\varphi}_f^T \boldsymbol{q}_f + \bar{\epsilon}_n \tau, \tag{12}$$

where $\bar{\epsilon}_N = \Sigma_{n=N+1}^{\infty} \omega_n^{-2} \psi_n \varphi_n$. (4) and (12) together form the finite dimensional approximation via the perturbed truncation of the modal model, that is, the perturbed truncation model.

The relative degree of the perturbed truncation model is equal to zero because τ appears in the output itself. Using the asymptotical expressions of the unconstrained modes again, we see that $\bar{\epsilon}_N = (-1)^{N+1} |O((N+1)^{-6})$ (see Appendix A) and the relative degree becomes ill-defined as the index N increases. The term $\bar{\epsilon}_N \tau$ can be viewed as the perturbations arising from the truncated high-order modes. Ignoring this term leads to the recovery of the finite dimensional approximation via the direct truncation and the relative degree jumps from zero to two. Let $\bar{r}(\bar{\epsilon}_N)$ and $\tilde{r}(\bar{\epsilon}_N)$ denote the relative degree of the perturbed truncation model and the direct truncation model, respectively. The above analysis results are summarized in Table I. In short, the perturbed truncation model exhibits the jumping behavior of the ill-defined relative degree.

Now we image four possible scenarios for the infinite dimensional system (2) with the tip output (3), which lead to four different finite dimensional approximations: the perturbed truncation model with $N > 0$, the direct truncation model with $N > 0$, the perturbed truncation model in the extreme case of $N=0$, the direct truncation model in the extreme case of $N=0$. From Table I we see that the perturbed parameter $\bar{\epsilon}_N$ decays to zero at a much faster rate than $\tilde{\epsilon}_N$ as the index N increases and the singularity effect is much worse than that in the second, so the first scenario is not computationally attractive for developing the inverse dynamics control design. Actually, as $N > 0$, the perturbed

Table I. Ill-defined behavior of the relative degree.

Truncation index N	0	$0 < N < \infty$	∞
$\bar{\epsilon}_N$	$\delta \omega_1^{-2} \psi_1 \varphi_1$	$(-1)^{N+1} \lvert O((N+1)^{-6}) \rvert$	0
$\tilde{\epsilon}_N$	$\psi_0 \varphi_0$	$(-1)^{N} \lvert O((N+1)^{-2}) \rvert$	0
$\bar{r}(\bar{\epsilon}_N)$	0	0	ill-defined
$\tilde{r}(\tilde{\epsilon}_N)$	2	2	ill-defined

https://doi.org/10.1017/S0263574701003526 Published online by Cambridge University Press

truncation model can be approximated well by ignoring the small perturbations as done in Hauser et al.;[32] this practice can make the first scenario degenerate to the second. Thus the second scenario rather than the first is justifiable for developing the inverse dynamics control design as done in the preceding literature. Unfortunately, the second scenario cannot predict the jumping behavior of the ill-defined relative degree. The third scenario can exhibit the jumping behavior of the ill-defined relative degree. This can be seen easily from the perturbed truncation model in the third scenario as

$$\ddot{q}_0 = \psi_0 \tau, \tag{13}$$

with the perturbed approximate output

$$\bar{y} = \varphi_0 q_0 + \bar{\epsilon}_0 \tau. \tag{14}$$

Moreover, note that $(-1)^n \omega_n^2 \psi_n \varphi_n > 0$ decreases strictly as n increases, thus there exists $0 < \delta < 1$ such that

$$\bar{\epsilon}_0 = \sum_{n=1}^{\infty} \omega_n^{-2} \psi_n \varphi_n = \delta \omega_1^{-2} \psi_1 \varphi_1 < 0.$$

It is straightforward that the system (13) with output (14) has an unstable zero. In other words, even in this extreme case, the nonminimum phase feature due to the flexibility can be retained in the perturbed truncation model. This is in contrast to the fourth scenario, where the rigid dynamics model is recovered excluding the flexible dynamics completely. Based on the above observations, the third scenario is not trivial but challenging. Thus it is necessary to explore potential advantages arising from the third scenario for the inverse dynamics control design. This will be done for a single-link flexible manipulator in the remainder of this section, and for a multi-link flexible manipulator in the next section.

2.4. Inverse dynamics control design

Based on the perturbed truncation model, the procedure for deriving the inverse dynamics is repeated as follows. With y_d instead of $\bar{y}$, inverting (12) gives

$$\bar{\tau}_d = \bar{\epsilon}_N^{-1}(y_d - \varphi_0 q_0 - \boldsymbol{\varphi}_f^T \boldsymbol{q}_f). \tag{15}$$

Substituting this into (4) yields

$$\begin{bmatrix} \ddot{q}_0 \\ \ddot{\boldsymbol{q}}_f \end{bmatrix} = \begin{bmatrix} -\bar{\epsilon}_N^{-1}\psi_0\varphi_0 & -\bar{\epsilon}_N^{-1}\psi_0\boldsymbol{\varphi}_f^T \\ -\bar{\epsilon}_N^{-1}\boldsymbol{\psi}_f\varphi_0 & -\boldsymbol{\Omega} - \bar{\epsilon}_N^{-1}\boldsymbol{\psi}_f\boldsymbol{\varphi}_f^T \end{bmatrix} \begin{bmatrix} q_0 \\ \boldsymbol{q}_f \end{bmatrix} + \bar{\epsilon}_N^{-1} \begin{bmatrix} \psi_0 \\ \boldsymbol{\psi}_f \end{bmatrix} y_d, \tag{16}$$

which is the internal dynamics. To distinguish from the solution of (4) again, $[\bar{q}_0\ \bar{\boldsymbol{q}}_f^T]^T$ denotes the solution of (16) later. Once the stable solution of (16) is found, the nominal torque is followed from (15). As mentioned above, we are interested in the inverse dynamics control design via the perturbed truncation in the extreme case of $N=0$. In this case, the internal dynamics (16) reduces to

$$\ddot{\bar{q}}_0 = \gamma \bar{q}_0 + \beta y_d, \tag{17}$$

where $\gamma = -\bar{\epsilon}_0^{-1}\psi_0\varphi_0 > 0$ and $\beta = \bar{\epsilon}_0^{-1}\psi_0$. Let $\boldsymbol{\eta} = [\bar{q}_0\ \ \dot{\bar{q}}_0]^T$. We can rewrite (17) as

$$\dot{\boldsymbol{\eta}} = \begin{bmatrix} 0 & 1 \\ \gamma & 0 \end{bmatrix} \boldsymbol{\eta} + \begin{bmatrix} 0 \\ \beta \end{bmatrix} y_d. \tag{18}$$

The requirement for a stable solution of (18) can be formulated as $\boldsymbol{\eta}(\pm\infty) = 0$. We explicitly find this bounded solution by first decomposing (18) into the acausal and causal decoupled form as

$$\dot{z}_{ac} = \gamma^{1/2} z_{ac} + \beta y_d/\sqrt{2},$$
$$\dot{z}_c = -\gamma^{1/2} z_c + \beta y_d/\sqrt{2},$$

where

$$\begin{bmatrix} z_{ac} \\ z_c \end{bmatrix} = \frac{1}{\sqrt{2}} \begin{bmatrix} \gamma^{1/2} & 1 \\ -\gamma^{1/2} & 1 \end{bmatrix} \boldsymbol{\eta},$$

and then integrating along the stable manifold forward in time, and backward along the unstable manifold to obtain the only stable solution as

$$z_{ac}(t) = \frac{1}{\sqrt{2}} \int_{-\infty}^{0} e^{\gamma^{1/2}\nu} \beta y_d(t-\nu)\, \mathrm{d}\nu,$$

$$z_c(t) = \frac{1}{\sqrt{2}} \int_{0}^{\infty} e^{-\gamma^{1/2}\nu} \beta y_d(t-\nu)\, \mathrm{d}\nu.$$

In short, for a given reference output $y_d(t) \in L_\infty(\mathbb{R})$, we can obtain the stable solution $\boldsymbol{\eta}$ as

$$\boldsymbol{\eta} = \begin{bmatrix} \bar{q}_0(t) \\ \dot{\bar{q}}_0(t) \end{bmatrix} = \begin{bmatrix} \gamma^{-1/2}(z_{ac}(t) - z_c(t))/\sqrt{2} \\ (z_{ac}(t) + z_c(t))/\sqrt{2} \end{bmatrix}.$$

Now we cast our case into the stable inversion based tracking control framework as follows. At the extreme case of $N=0$, (15) becomes

$$\bar{\tau}_d = \bar{\epsilon}_0^{-1}(y_d - \varphi_0 \bar{q}_0),$$

which can be used to generate the bounded nominal torque trajectory as the feedforward input when we obtain the stable solution $\bar{q}_0$ of the internal dynamics (17) for a given reference output $y_d(t)$. At this off-line stage, all fast transients of the flexible dynamics are ignored in the perturbed truncation model; thus, the error dynamics arises[27] and needs to be stabilized for preventing the so-called control spillover phenomenon.[33] We can merge this task into the online feedback stabilizing stage. Note that the quasi-steady-states of the fast modes are almost constant during fast transient, that is, $\dot{\bar{q}}_n = \ddot{\bar{q}}_n = 0$, $n \geq 1$. Let τ_e denote the additional torque that is used to stabilize the error dynamics. Applying $\tau = \bar{\tau}_d + \tau_e$ to the tip tracking control system (2) yields the error dynamics of

$$\ddot{e}_n + \omega_n^2 e_n = \psi_n \tau_e, \tag{19}$$

where $e_n = q_n - \bar{q}_n$. The resulting tip tracking error can be expressed by

$$y_e = \sum_{n=0}^{\infty} \psi_n e_n. \tag{20}$$

https://doi.org/10.1017/S0263574701003526 Published online by Cambridge University Press

Recall (1) and note that $\bar{\theta}=\sum_{n=0}^{\infty}\bar{q}_n\psi_n$ and $\theta=\sum_{n=0}^{\infty}q_n\psi_n$. Let $\theta_e=\theta-\bar{\theta}$. For any $k_p>0$, consider the following energy based Lyapunov function

$$V=\frac{1}{2}\theta_e^2k_p+\frac{1}{2}\sum_{n=1}^{\infty}e_n^2\omega_n^2+\frac{1}{2}\sum_{n=0}^{\infty}\dot{e}_n^2.$$

Time differentiation of this function is

$$\dot{V}=\dot{\theta}_ek_p\theta_e+\sum_{n=0}^{\infty}\dot{e}_n(e_n\omega_n^2+\ddot{e}_n)$$

$$=\dot{\theta}_ek_p\theta_e+\left(\sum_{n=0}^{\infty}\dot{e}_n\psi_n\right)\tau_e$$

$$=\dot{\theta}_e(k_p\theta_e+\tau_e).$$

We take the feedback control law as

$$\tau_e=-k_p\theta_e-k_d\dot{\theta}_e, \tag{21}$$

where $k_d>0$, this leads to

$$\dot{V}(t)=-k_d\dot{\theta}_e^2<0.$$

This means that the error dynamics can be asymptotically stabilized by the joint-based PD type feedback law in (21), that is, for each n, $e_n(t)\to 0$ as $t\to\infty$, thus $y_e(t)\to 0$ as $t\to\infty$.

Before ending this section, we make the following remark. Based on the perturbed truncation model, the inverse dynamics control design can be used to track not so much trajectories, especially, being unnecessarily twice differentiable. That is, finding the bounded nominal torque $\tau_d(t)\in L_\infty(\mathbb{R})$ only requires that the reference output $y_d(t)$ is in $L_\infty(\mathbb{R})$.[8] This is different from the situation via the direct truncation that requires $y_d(t)$ to be necessarily twice differentiable and $y_d^{(2)}(t)$ in $L_\infty(\mathbb{R})$ (as required by a rigid system). This advantage attributes to the link flexibility. In the next section, the further potential advantages arising from the perturbed truncation model in this extreme case will be explored for the inverse dynamics control design of a multi-link flexible manipulator.

3. MAIN RESULTS FOR MULTI-LINK FLEXIBLE MANIPULATOR

3.1. System description

Consider an open kinematic chain structure, with a fixed base and N moving flexible links, interconnected by revolute joints. To model the flexible manipulator, all links are assumed to be uniform slender beams that satisfy the assumption of Euler-Bernoulli beam theory and link flexibility is limited to the plane of nominal rigid motion. For the i-th link, the deflection in the i-th rotating frame can be expressed by modal expansion as

$$w_i(t,x_i)=\sum_{j=1}^{m_i}q_{ij}(t)\phi_{ij}(x_i),\ 0\le x_i\le l_i,$$

where $\{\phi_{ij}(x_i)\}_{j=1}^{m_i}$ are the orthogonal normalized clamped modes of link i, l_i is the length of link i. Define the vector of generalized coordinate $\boldsymbol{q}$ as

$$\boldsymbol{q}=\overbrace{q_{10}\ldots q_{N0}}^{\boldsymbol{q}_0^T}\ \underbrace{q_{11}\ldots q_{1m_1}\ldots q_{N1}\ldots q_{Nm_N}}_{\boldsymbol{q}_f^T}]^T=[\boldsymbol{q}_0^T\ \boldsymbol{q}_f^T]^T.$$

Here $\boldsymbol{q}_0\in\mathbb{R}^N$ is the vector of N joint angles and $\boldsymbol{q}_f\in\mathbb{R}^{N_f}$ is the vector of N_f flexible coordinates, and $N_f=\sum_{j=1}^{N}m_j$. Ignoring the joint viscous friction and gravitational effects, the dynamics of the multi-link flexible manipulator are governed by the following motion equation

$$\boldsymbol{H}(\boldsymbol{q})\ddot{\boldsymbol{q}}+\boldsymbol{K}_e\boldsymbol{q}+\boldsymbol{D}_e\dot{\boldsymbol{q}}+\boldsymbol{H}_c(\boldsymbol{q},\dot{\boldsymbol{q}})=\boldsymbol{B}\boldsymbol{\tau}, \tag{22}$$

or

$$\begin{bmatrix}\boldsymbol{H}_{00}(\boldsymbol{q}_0,\boldsymbol{q}_f) & \boldsymbol{H}_{0f}(\boldsymbol{q}_0,\boldsymbol{q}_f)\\ \boldsymbol{H}_{0f}^T(\boldsymbol{q}_0,\boldsymbol{q}_f) & \boldsymbol{H}_{ff}(\boldsymbol{q}_0,\boldsymbol{q}_f)\end{bmatrix}\begin{bmatrix}\ddot{\boldsymbol{q}}_0\\ \ddot{\boldsymbol{q}}_f\end{bmatrix}+\begin{bmatrix}\boldsymbol{0} & \boldsymbol{0}\\ \boldsymbol{0} & \boldsymbol{K}\end{bmatrix}\begin{bmatrix}\boldsymbol{q}_0\\ \boldsymbol{q}_f\end{bmatrix}$$

$$+\begin{bmatrix}\boldsymbol{0} & \boldsymbol{0}\\ \boldsymbol{0} & \boldsymbol{D}\end{bmatrix}\begin{bmatrix}\dot{\boldsymbol{q}}_0\\ \dot{\boldsymbol{q}}_f\end{bmatrix}+\begin{bmatrix}\boldsymbol{H}_{c0}(\boldsymbol{q}_0,\boldsymbol{q}_f,\dot{\boldsymbol{q}}_0,\dot{\boldsymbol{q}}_f)\\ \boldsymbol{H}_{cf}(\boldsymbol{q}_0,\boldsymbol{q}_f,\dot{\boldsymbol{q}}_0,\dot{\boldsymbol{q}}_f)\end{bmatrix}=\begin{bmatrix}\boldsymbol{I}\\ \boldsymbol{0}\end{bmatrix}\boldsymbol{\tau}, \tag{23}$$

where $\boldsymbol{I}$ is an $N\times N$ identity matrix, $\boldsymbol{\tau}$ is the vector of the joint torques, $\boldsymbol{H}(\boldsymbol{q})$, $\boldsymbol{K}_e$ and $\boldsymbol{D}_e$ are the generalized inertia matrix, stiffness matrix and damping matrix, respectively. $\boldsymbol{H}_c(\boldsymbol{q},\dot{\boldsymbol{q}})$ is the vector of the generalized Coriolis and centrifugal forces, which can be expressed as

$$\boldsymbol{H}_c(\boldsymbol{q},\dot{\boldsymbol{q}})=\dot{\boldsymbol{H}}(\boldsymbol{q})\dot{\boldsymbol{q}}-\frac{1}{2}\frac{\partial}{\partial\boldsymbol{q}}(\dot{\boldsymbol{q}}^T\boldsymbol{H}(\boldsymbol{q})\dot{\boldsymbol{q}})=\boldsymbol{C}(\boldsymbol{q},\dot{\boldsymbol{q}})\dot{\boldsymbol{q}}.$$

We assume that the above motion equation is derived from the system Lagrangian. Some well-known properties of this dynamic model under the small deformation assumption are listed in Appendix B.

Here the net displacement of each link is used as the output variable. Define

$$\boldsymbol{\varphi}_0=\mathrm{diag}(l_1,l_2,\ldots,l_N),$$

$$\boldsymbol{\varphi}_f=\mathrm{diagblock}(\boldsymbol{\varphi}_1,\boldsymbol{\varphi}_2,\ldots,\boldsymbol{\varphi}_N),$$

where $\boldsymbol{\varphi}_i=[\phi_{i1}(l_i)\phi_{i2}(l_i)\ldots\phi_{im_i}(l_i)]^T$, $i=1,2,\ldots,N$. Then the output can be expressed as

$$\boldsymbol{y}=\boldsymbol{\Phi}_0\boldsymbol{q}_0+\boldsymbol{\Phi}_f^T\boldsymbol{q}_f. \tag{25}$$

3.2. Inverse dynamics

In this section, the inverse dynamics based on the perturbed truncation model in the extreme case of $N=0$ for the single-link flexible manipulator is extended to the multi-link flexible manipulator described above. The procedure of doing this is outlined as follows: Firstly, we construct the perturbed truncation model in the extreme case of truncating

https://doi.org/10.1017/S0263574701003526 Published online by Cambridge University Press

all of the flexible modes. Then the issue of the inverse dynamics is reformulated based on this perturbed truncation model for generating a feedforward command. Finally, potential advantages arising from this novel formulation are discussed.

According to the multi-time-scale characteristics, the generalized coordinate vector $\boldsymbol{q}$ is partitioned into two groups: the slow part $\boldsymbol{q}_0$ (rigid modes) and the fast part $\boldsymbol{q}_f$ (flexible modes). Again based on the singular perturbation analysis,[27] (23) can be represented as the singular perturbation form of

$$\begin{aligned}\boldsymbol{H}_{00}(\boldsymbol{q}_0, \boldsymbol{\mu}^2\boldsymbol{\xi}_f)\ddot{\boldsymbol{q}}_0+\boldsymbol{H}_{0f}(\boldsymbol{q}_0, \boldsymbol{\mu}^2\boldsymbol{\xi}_f)\boldsymbol{\mu}^2\ddot{\boldsymbol{\xi}}_f\\ +\boldsymbol{H}_{c0}(\boldsymbol{q}_0, \boldsymbol{\mu}^2\boldsymbol{\xi}_f, \dot{\boldsymbol{q}}_0, \boldsymbol{\mu}^2\dot{\boldsymbol{\xi}}_f)=\boldsymbol{\tau},\end{aligned} \tag{26}$$

$$\begin{aligned}\boldsymbol{H}_{0f}^T(\boldsymbol{q}_0, \boldsymbol{\mu}^2\boldsymbol{\xi}_f)\ddot{\boldsymbol{q}}_0+\boldsymbol{H}_{ff}(\boldsymbol{q}_0, \boldsymbol{\mu}^2\boldsymbol{\xi}_f)\boldsymbol{\mu}^2\ddot{\boldsymbol{\xi}}_f+\boldsymbol{\xi}_f+\boldsymbol{D}\boldsymbol{\mu}^2\dot{\boldsymbol{\xi}}_f\\ +\boldsymbol{H}_{cf}(\boldsymbol{q}_0, \boldsymbol{\mu}^2\boldsymbol{\xi}_f, \dot{\boldsymbol{q}}_0, \boldsymbol{\mu}^2\dot{\boldsymbol{\xi}}_f)=\boldsymbol{0},\end{aligned} \tag{27}$$

where $\boldsymbol{\mu}^2=\boldsymbol{K}^{-1}$ is also diagonal and its diagonal elements are the time scalars or the singular perturbation parameters, and $\boldsymbol{q}_f=\boldsymbol{\mu}^2\boldsymbol{\xi}_f$. Making $\boldsymbol{\mu}=\boldsymbol{0}$ in (26) and (27) results in the following degenerated form

$$\boldsymbol{H}_{00}(\bar{\boldsymbol{q}}_0)\ddot{\bar{\boldsymbol{q}}}_0+\boldsymbol{H}_{c0}(\bar{\boldsymbol{q}}_0, \dot{\bar{\boldsymbol{q}}}_0)=\boldsymbol{\tau}, \tag{28}$$

$$\boldsymbol{H}_{0f}^T(\bar{\boldsymbol{q}}_0)\ddot{\bar{\boldsymbol{q}}}_0+\bar{\boldsymbol{\xi}}_f+\boldsymbol{H}_{cf}(\bar{\boldsymbol{q}}_0,\dot{\bar{\boldsymbol{q}}}_0)=\boldsymbol{0}, \tag{29}$$

which are the first-order approximations to (26) and (27) with respect to the perturbation parameters. Solving for $\ddot{\bar{\boldsymbol{q}}}_0$ from (28) and substituting it into (29) yields

$$\bar{\boldsymbol{\xi}}_f=\boldsymbol{H}_{0f}^T(\bar{\boldsymbol{q}}_0)\boldsymbol{H}_{00}^{-1}(\bar{\boldsymbol{q}}_0)(\boldsymbol{H}_{c0}(\bar{\boldsymbol{q}}_0, \dot{\bar{\boldsymbol{q}}}_0)-\boldsymbol{\tau})-\boldsymbol{H}_{cf}(\bar{\boldsymbol{q}}_0, \dot{\bar{\boldsymbol{q}}}_0). \tag{30}$$

As done for a single-link manipulator, $\boldsymbol{q}_f$ is approximated by

$$\begin{aligned}\boldsymbol{q}_f \approx \bar{\boldsymbol{q}}_f=\boldsymbol{K}^{-1}\boldsymbol{H}_{0f}^T(\bar{\boldsymbol{q}}_0)\boldsymbol{H}_{00}^{-1}(\bar{\boldsymbol{q}}_0)(\boldsymbol{H}_{c0}(\bar{\boldsymbol{q}}_0, \dot{\bar{\boldsymbol{q}}}_0)-\boldsymbol{\tau})\\ -\boldsymbol{K}^{-1}\boldsymbol{H}_{cf}(\bar{\boldsymbol{q}}_0, \dot{\bar{\boldsymbol{q}}}_0).\end{aligned} \tag{31}$$

Substituting (31) into (25) gives the perturbed approximation to the output as

$$\bar{\boldsymbol{y}}=\boldsymbol{\Phi}_0\bar{\boldsymbol{q}}_0+\boldsymbol{\alpha}(\bar{\boldsymbol{q}}_0, \dot{\bar{\boldsymbol{q}}}_0)+\boldsymbol{\epsilon}(\bar{\boldsymbol{q}}_0)\boldsymbol{\tau}, \tag{32}$$

where

$$\boldsymbol{\epsilon}(\bar{\boldsymbol{q}}_0)=-\boldsymbol{\Phi}_f^T\boldsymbol{K}^{-1}\boldsymbol{H}_{0f}^T(\bar{\boldsymbol{q}}_0)\boldsymbol{H}_{00}^{-1}(\bar{\boldsymbol{q}}_0), \tag{33}$$

$$\boldsymbol{\alpha}(\bar{\boldsymbol{q}}_0, \dot{\bar{\boldsymbol{q}}}_0)=-\boldsymbol{\epsilon}(\bar{\boldsymbol{q}}_0)\boldsymbol{H}_{c0}(\bar{\boldsymbol{q}}_0, \dot{\bar{\boldsymbol{q}}}_0)-\boldsymbol{\Phi}_f^T\boldsymbol{K}^{-1}\boldsymbol{H}_{cf}(\bar{\boldsymbol{q}}_0, \dot{\bar{\boldsymbol{q}}}_0). \tag{34}$$

Until now (28) with the perturbed output (32) forms the perturbed truncation model in the extreme case of truncating all of the flexible modes. Before the inverse dynamics control design is developed, the relative degree of this perturbed truncation model needs to be checked. We trivially assume that $\boldsymbol{H}_{0f}(\bar{\boldsymbol{q}}_0)$ is a full-rank matrix. The logic behind this assumption is that any rigid motion can cause the link deformation; this is clearly consistent with mechanical intuition. Thus the matrix $\boldsymbol{\epsilon}(\bar{\boldsymbol{q}}_0)$ is nonsingular and the relative degree is uniform for all output variables and equal to zero. Ignoring the perturbation term $\boldsymbol{\epsilon}(\bar{\boldsymbol{q}}_0)\boldsymbol{\tau}$ in (32) leads to the relative degree jumping from zero to two as the situation of a single-link flexible manipulator.

With a given reference output $\boldsymbol{y}_d$ instead of $\bar{\boldsymbol{y}}$, inverting (32) gives

$$\bar{\boldsymbol{\tau}}_d=\boldsymbol{\epsilon}^{-1}(\bar{\boldsymbol{q}}_0)\,(\boldsymbol{y}_d-\boldsymbol{\Phi}_0\bar{\boldsymbol{q}}_0-\boldsymbol{\alpha}(\bar{\boldsymbol{q}}_0, \dot{\bar{\boldsymbol{q}}}_0)). \tag{35}$$

Substituting this into (28) yields the internal dynamics as

$$\ddot{\bar{\boldsymbol{q}}}_0=\boldsymbol{\Gamma}(\bar{\boldsymbol{q}}_0)\bar{\boldsymbol{q}}_0+\boldsymbol{\sigma}(\bar{\boldsymbol{q}}_0, \dot{\bar{\boldsymbol{q}}}_0)+\boldsymbol{\beta}(\bar{\boldsymbol{q}}_0)\boldsymbol{y}_d, \tag{36}$$

where

$$\boldsymbol{\beta}(\bar{\boldsymbol{q}}_0)=\boldsymbol{H}_{00}^{-1}(\bar{\boldsymbol{q}}_0)\boldsymbol{\epsilon}^{-1}(\bar{\boldsymbol{q}}_0)=-(\boldsymbol{\Phi}_f^T\boldsymbol{K}^{-1}\boldsymbol{H}_{0f}^T(\bar{\boldsymbol{q}}_0))^{-1}, \tag{37}$$

$$\boldsymbol{\Gamma}(\bar{\boldsymbol{q}}_0)=-\boldsymbol{\beta}(\bar{\boldsymbol{q}}_0)\boldsymbol{\Phi}_0, \tag{38}$$

$$\boldsymbol{\sigma}(\bar{\boldsymbol{q}}_0,\dot{\bar{\boldsymbol{q}}}_0)=\boldsymbol{\beta}(\bar{\boldsymbol{q}}_0)\boldsymbol{\Phi}_f^T\boldsymbol{K}^{-1}\boldsymbol{H}_{cf}(\bar{\boldsymbol{q}}_0, \dot{\bar{\boldsymbol{q}}}_0). \tag{39}$$

Again, the stable solution of (36) must be firstly sought for calculating the nominal torque by (35). At this stage, potential advantages arising from this novel formulation are emphasized via the following remarks.

Remark 1. In the existing formulation of the inverse dynamics of a multi-link flexible manipulator, the internal dynamics is a completely fast (flexible) dynamic model driven by a reference trajectory being necessarily twice differentiable. Also, the response of this fast internal dynamics can cause high-frequency saturation effects that deteriorate tracking performance. In this new formulation, the internal dynamics given by (36) is a slow but slightly nonminimum phase (rigid) dynamic model driven by a reference trajectory being unnecessarily twice differentiable. Moreover, this internal dynamics excludes the fast transients of the flexible dynamics and its behavior is well-conditioned at high frequencies so that high-frequency saturation effects can be alleviated.

Remark 2. In the existing formulation of the inverse dynamics, the order of the internal dynamics is equal to the total truncation number N_f of the flexible modes. But in this new formulation, the order of this internal dynamics is always the same as the link number N which is usually lower than N_f.

Remark 3. There are two main difficulties in solving bounded solution of the internal dynamics in existing formulation of the inverse dynamics of a multi-link flexible manipulator. One is the nonlinearities due to the strongly nonlinear forward dynamics, another is the configuration-dependent time-varying feature. In what follows, we show that this new formulation of the inverse dynamics leads to a nearly linear and time-invariant internal dynamics, thus the computation of solving bounded solutions of the inverse dynamics becomes efficient.

Actually, when the matrix $\boldsymbol{H}_{0f}(\bar{\boldsymbol{q}}_0)$ is slowly time-varying, a rather common practice is to approximate it by a constant matrix $\hat{\boldsymbol{H}}_{0f}$ under the small deformation assumption.[24] In this case, it follows from (24) that

$$\boldsymbol{H}_{cf}(\bar{\boldsymbol{q}}_0, \dot{\bar{\boldsymbol{q}}}_0)=\dot{\boldsymbol{H}}_{0f}^T(\bar{\boldsymbol{q}}_0)\dot{\bar{\boldsymbol{q}}}_0\approx\boldsymbol{0},$$

thus $\boldsymbol{\sigma}(\bar{\boldsymbol{q}}_0, \dot{\bar{\boldsymbol{q}}}_0)\approx\boldsymbol{0}$. Then the internal dynamics (36) can be approximated by the time-invariant linear system in the form of

$$\ddot{\bar{\boldsymbol{q}}}_0=\hat{\boldsymbol{\Gamma}}\bar{\boldsymbol{q}}_0+\hat{\boldsymbol{\beta}}\boldsymbol{y}_d, \tag{40}$$

where $\hat{\boldsymbol{\beta}}=-(\boldsymbol{\Phi}_f^T\boldsymbol{K}^{-1}\hat{\boldsymbol{H}}_{0f}^T)^{-1}$ and $\hat{\boldsymbol{\Gamma}}=-\hat{\boldsymbol{\beta}}\boldsymbol{\Phi}_0$. It is natural to expect that the internal dynamics (40) has unstable poles like the situation of a single-link flexible manipulator, thus

https://doi.org/10.1017/S0263574701003526 Published online by Cambridge University Press

we assume that $\hat{\mathbf{\Gamma}}$ is positive definite and noncausal bounded solutions must be sought. Let $\boldsymbol{\eta}=[\hat{\boldsymbol{q}}_0^T\ \dot{\hat{\boldsymbol{q}}}_0^T]^T$. We can rewrite (40) as

$$\dot{\boldsymbol{\eta}}=\begin{bmatrix}\mathbf{0} & \boldsymbol{I}\\ \hat{\mathbf{\Gamma}} & \mathbf{0}\end{bmatrix}\boldsymbol{\eta}+\begin{bmatrix}\mathbf{0}\\ \hat{\boldsymbol{\beta}}\end{bmatrix}\boldsymbol{y}_d. \tag{41}$$

The requirement for a stable solution of (41) can be formulated as $\boldsymbol{\eta}(\pm\infty)=\mathbf{0}$. Again, we explicitly find a bounded solution by first decomposing (41) in the acausal and causal decoupled form as

$$\dot{\boldsymbol{z}}_{ac}=\hat{\mathbf{\Gamma}}^{1/2}\boldsymbol{z}_{ac}+\hat{\boldsymbol{\beta}}\boldsymbol{y}_d/\sqrt{2},$$
$$\dot{\boldsymbol{z}}_{c}=-\hat{\mathbf{\Gamma}}^{1/2}\boldsymbol{z}_{c}+\hat{\boldsymbol{\beta}}\boldsymbol{y}_d/\sqrt{2},$$

where

$$\begin{bmatrix}\boldsymbol{z}_{ac}\\ \boldsymbol{z}_{c}\end{bmatrix}=\frac{1}{\sqrt{2}}\begin{bmatrix}\hat{\mathbf{\Gamma}}^{1/2} & \boldsymbol{I}\\ -\hat{\mathbf{\Gamma}}^{1/2} & \boldsymbol{I}\end{bmatrix}\boldsymbol{\eta}$$

and then integrating along the stable manifold forward in time, and backward along the unstable manifold to obtain the only stable solution as

$$\boldsymbol{z}_{ac}(t)=\frac{1}{\sqrt{2}}\int_{-\infty}^{0} e^{\hat{\mathbf{\Gamma}}^{1/2}\nu}\hat{\boldsymbol{\beta}}\boldsymbol{y}_d(t-\nu)\,\mathrm{d}\nu,$$

$$\boldsymbol{z}_{c}(t)=\frac{1}{\sqrt{2}}\int_{0}^{\infty} e^{-\hat{\mathbf{\Gamma}}^{1/2}\nu}\hat{\boldsymbol{\beta}}\boldsymbol{y}_d(t-\nu)\,\mathrm{d}\nu.$$

Vector $\boldsymbol{\eta}(t)$ can be obtained by

$$\boldsymbol{\eta}=\begin{bmatrix}\hat{\boldsymbol{q}}_0(t)\\ \dot{\hat{\boldsymbol{q}}}_0(t)\end{bmatrix}=\begin{bmatrix}\hat{\mathbf{\Gamma}}^{-1/2}(\boldsymbol{z}_{ac}(t)-\boldsymbol{z}_c(t))/\sqrt{2}\\ (\boldsymbol{z}_{ac}(t)+\boldsymbol{z}_c(t))/\sqrt{2}\end{bmatrix}.$$

Then the nominal torque $\hat{\boldsymbol{\tau}}_d$ follows from the approximation form of (35), that is,

$$\hat{\boldsymbol{\tau}}_d=\hat{\boldsymbol{\epsilon}}^{-1}(\hat{\boldsymbol{q}}_0)(\boldsymbol{y}_d-\boldsymbol{\Phi}_0\hat{\boldsymbol{q}}_0)+\boldsymbol{H}_{c0}(\hat{\boldsymbol{q}}_0,\dot{\hat{\boldsymbol{q}}}_0), \tag{42}$$

where

$$\hat{\boldsymbol{\epsilon}}(\hat{\boldsymbol{q}}_0)=-\boldsymbol{\Phi}_f^T\boldsymbol{K}^{-1}\hat{\boldsymbol{H}}_{0f}^T\boldsymbol{H}_{00}^{-1}(\hat{\boldsymbol{q}}_0).$$

If needed, based on the above approximation formulation the internal dynamics (36) can be solved iteratively as done in Hunt and Meyer[9]

$$\bar{\boldsymbol{q}}_0^1=\hat{\boldsymbol{q}}_0, \tag{43}$$

$$\ddot{\bar{\boldsymbol{q}}}_0^{k+1}=\hat{\mathbf{\Gamma}}\bar{\boldsymbol{q}}_0^{k+1}+\boldsymbol{s}(\bar{\boldsymbol{q}}_0^k,\dot{\bar{\boldsymbol{q}}}_0^k,\boldsymbol{y}_d),\ k\geq 1 \tag{44}$$

where

$$\boldsymbol{s}(\bar{\boldsymbol{q}}_0^k,\dot{\bar{\boldsymbol{q}}}_0^k,\boldsymbol{y}_d)=(\mathbf{\Gamma}(\bar{\boldsymbol{q}}_0^k)-\hat{\mathbf{\Gamma}})\bar{\boldsymbol{q}}_0^k+\boldsymbol{\sigma}(\bar{\boldsymbol{q}}_0^k,\dot{\bar{\boldsymbol{q}}}_0^k)+\boldsymbol{\beta}(\bar{\boldsymbol{q}}_0^k)\boldsymbol{y}_d.$$

The noncausal bounded solution for (44) can be found in the same way as solving (40). Recall (37)–(39), the above perturbation term $\boldsymbol{s}(\bar{\boldsymbol{q}}_0^k,\dot{\bar{\boldsymbol{q}}}_0^k,\boldsymbol{y}_d)$ is nearly linear and slowly time-varying and the uniformly Lipschitz condition[9] is easily satisfied so that the above iterative process can be guaranteed to converge the solution of the internal dynamics (36) for most practical applications.

Similarly as in the case of a single-link flexible manipulator, we need to stabilize the error dynamics arising from the approximation via the perturbed truncation. In Appendix B, we show that the joint-based PD type feedback control integrated with the passive control provided by the structure stiffness and damping can be used to stabilize the error dynamics locally. It should be noted that much sophisticated analysis and design procedures should be sought if the structure passive control is not available. This is out of the focus of this paper.

As a summary of this section, we assert that there are two potential advantages arising from the above formulation of the inverse dynamics. First, like in the case of a single-link flexible arm, the inverse dynamics control design developed here can be used to track trajectories being unnecessarily twice differentiable. Thus the solution holds great promise to a much wider range of practical applications. Second, this new formulation leads to nearly linear and time-invariant internal dynamics with a relatively lower order, its simplicity makes the inverse dynamics control design practically useful.

4. NUMERICAL SIMULATION FOR CASE STUDIES

To demonstrate the potential advantages arising from the perturbed truncation model for the inverse dynamics control design, numerical simulation studies are conducted for the two cases. One case is a planar single-link flexible arm. In this case, we intend to illustrate the ill-defined jumping behavior of the relative degree and compare the inverse dynamics based on the perturbed truncation model with that based on the direct truncation model. Another case is a planar elbow arm. This case study is expected to provide a basic understanding of the inverse dynamics control design based on the perturbed truncation model for more complex systems. These two experimental setups have been developed at the control engineering laboratory of Ruhr-University Bochum.[21] The extended experimental studies will be reported later.

4.1. A planar single-link flexible arm

The implementation of the simulation requires the following basic parameters: $l=0.92$ m, $EI=15.75$ N.m^2, $\rho=0.81$ kg/m, $J_h=1.081$ kg.m^2, $M_t=0.412$ kg. Table II lists the calculated values of the modal parameters ω_n^2, φ_n and ψ_n.

The asymptotic behavior between $\tilde{\boldsymbol{\epsilon}}_N$ and $\bar{\boldsymbol{\epsilon}}_N$ with respect to the truncation index N is compared in Table III. These numerical results confirm the analysis results on the jumping behavior of the ill-defined relative degree. In

Table II. Modal parameters of flexible beam.

Mode index	ω_n^2	φ_n	ψ_n
0	0	0.7184	0.7809
1	1.5480×10^2	1.0861	−0.5538
2	7.7114×10^3	−0.5600	−0.0862
3	7.2206×10^4	0.3619	−0.0283
4	3.0446×10^5	−0.2628	−0.0138
5	8.7906×10^5	0.2061	−0.0081

https://doi.org/10.1017/S0263574701003526 Published online by Cambridge University Press

Table III. Asymptotic behavior of perturbation parameters.

Truncation index	$\tilde{\epsilon}_N$	$\bar{\epsilon}_N$
0	5.6099×10^{-1}	-3.8798×10^{-3}
1	-4.0599×10^{-2}	6.1293×10^{-6}
2	7.7241×10^{-3}	-1.3198×10^{-7}
3	-2.5298×10^{-3}	1.0030×10^{-8}
4	1.1053×10^{-3}	-1.9101×10^{-9}

addition, except in the extreme case of $N=0$, there is little difference between the models via the perturbed truncation and the direct truncation because $\bar{\epsilon}_N$ is too small.

At first, we consider two cases for the trajectories to be tracked, which are shown in Figure 2. The first is a typical Bang-Bang profile with the starting time $t_s=0.4$ s and the final time $t_f=2.8$ s. We are interested in it because it contains significant high-frequency contents. Another is a smooth profile generated by

$$y_d^{(4)}(t)=y_d^{(3)}(t)=y_d^{(2)}(t)=y_d^{(1)}(t)=y_d(t)=0,\ t<0.4,$$
$$y_d^{(5)}(t)+29.75y_d^{(4)}(t)+354.03y_d^{(3)}(t)+2088y_d^{(2)}(t)+$$
$$6264.1y_d^{(1)}(t)+7543y_d(t)-7543=0,\ t\geq 0.4$$

For these two command trajectories, the inverse dynamics based on the perturbed truncation model in the extreme case of $N=0$ and the direct truncation model in the case of $N=1$ are used to produce the calculated torque trajectories shown in Figure 3. We denote them as the perturbed and unperturbed torque for simplicity.

Then these calculated torque trajectories are applied to drive the flexible manipulator as feedforward commands; the tracking errors are plotted in Figure 4. In case 1, the perturbed torque works much better than the unperturbed torque; this is not surprising, as the direct truncation model even in the case of $N=1$ leads to the ill-conditioned inverse dynamics at high frequencies;[17] the high-frequency contents contained in the bang-bang profiles cause high-frequency saturation effects that deteriorate tracking performance, while the perturbed truncation model excludes the fast transient of the flexible dynamics and the resulting inverse dynamics is well-conditioned at high frequencies and no high-frequency saturation effects occur. The situation in case 2 is in contrast to that in case 1. The smoothing trajectory to be tracked alleviates the high-frequency saturation effects and makes the direct truncation model more close to the original system than the perturbed truncation model so that a better tracking performance is achieved by the unperturbed torque.

To understand the ability of tracking trajectories being unnecessarily twice differentiable, the following tip reference trajectory is considered:

$$\dot{y}_d(t)=\begin{cases} 0 & 0\leq t<0.4 \\ v_0 & 0.4\leq t<1.4 \\ v_0/4 & 1.4\leq t<2.2 \\ v_0/8 & 2.2\leq t<2.6 \\ v_0/16 & 2.6\leq t<2.8 \\ 0 & 2.8\leq t\leq 3.2 \end{cases}$$

where $v_0=0.3125$[m/sec]. The perturbed torque profile is shown in the top of Figure 5, and the comparison result on the tip tracking in the bottom. As expected, there exist some

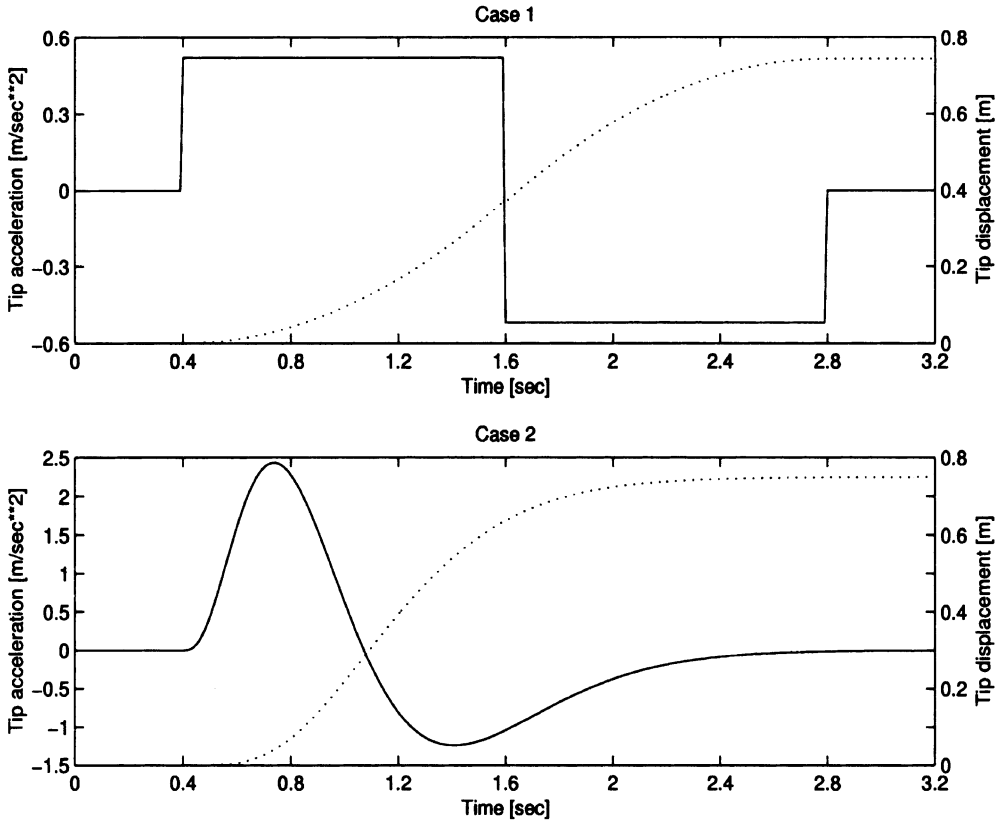

Fig. 2. Reference tip trajectories: (top) case 1; (bottom) case 2; solid line for acceleration; dotted line for displacement.

https://doi.org/10.1017/S0263574701003526 Published online by Cambridge University Press

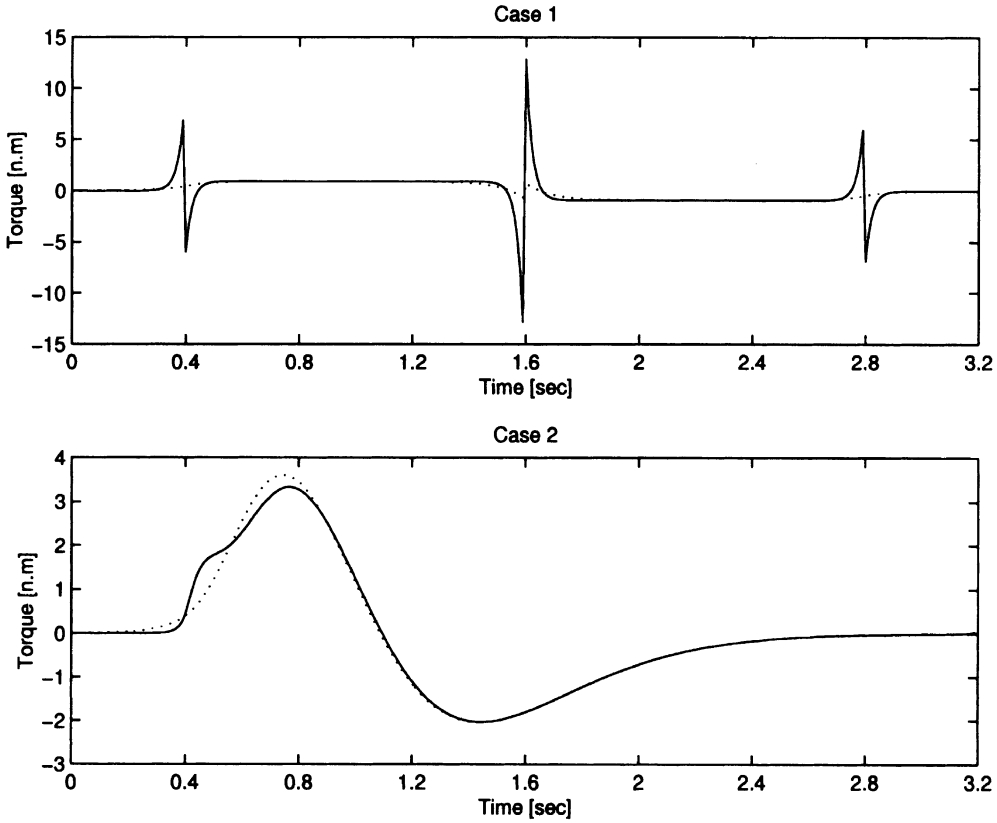

Fig. 3. Comparison results of the calculated torque: (top) case 1; (bottom) case 2; solid line for the direct truncation model with $N=1$; dotted line for the perturbed truncation model with $N=0$.

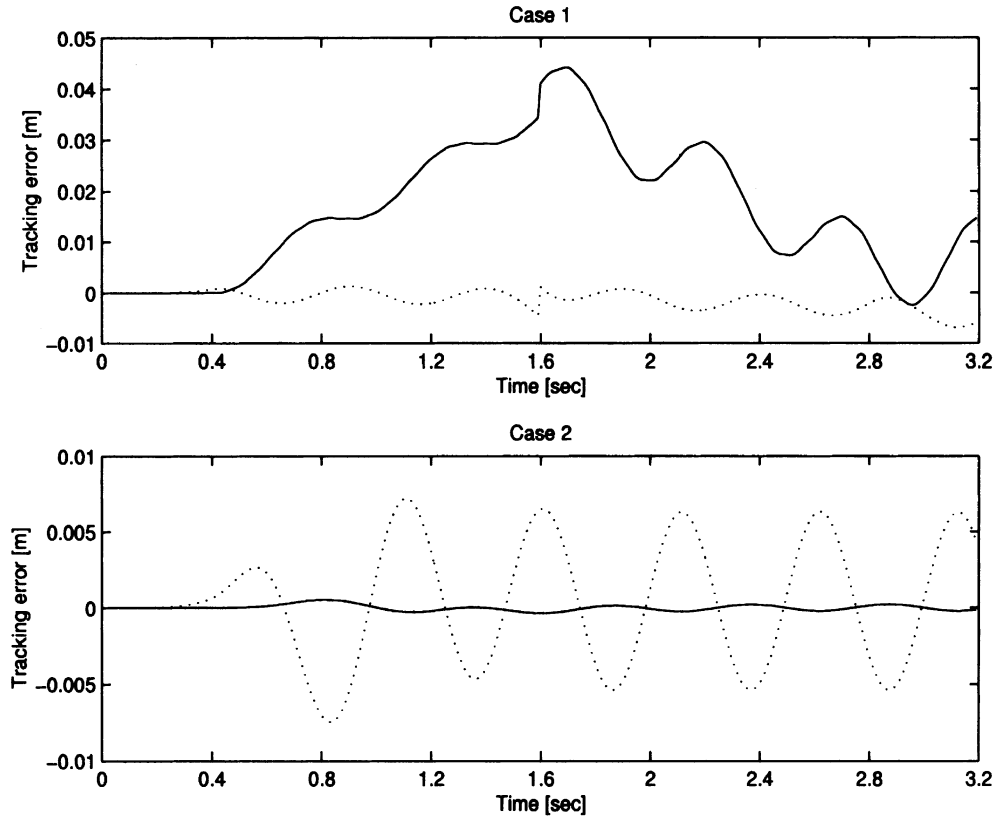

Fig. 4. Comparison results of the tracking errors: (top) case 1; (bottom) case 2; solid line for the direct truncation model with $N=1$; dotted line for the perturbed truncation model with $N=0$.

https://doi.org/10.1017/S0263574701003526 Published online by Cambridge University Press

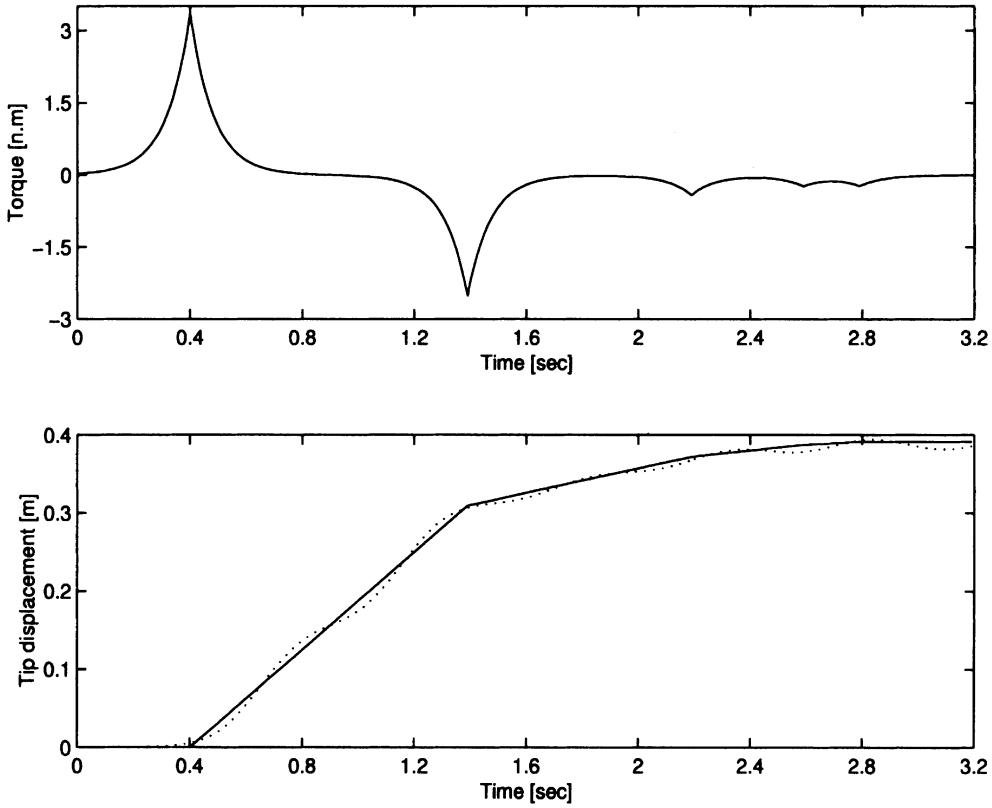

Fig. 5. Tracking trajectory without twice differentiation: (top) calculated torque; (bottom) tip displacement profiles (solid line for the reference trajectory).

peaks in the calculated torque trajectory at the discontinuous points of the tip velocity. This calculated torque can drive the tip of the flexible manipulator to follow smoothly and swing slightly along the given tip reference trajectory.

4.2. A planar elbow manipulator

This section consider a planar elbow manipulator to track the desired endpoint motion of the *x*-component line movement shown in Figure 6. The basic link parameters are listed in Table IV for an ideal model from which the perturbed truncation based inverse dynamics control design can be developed.

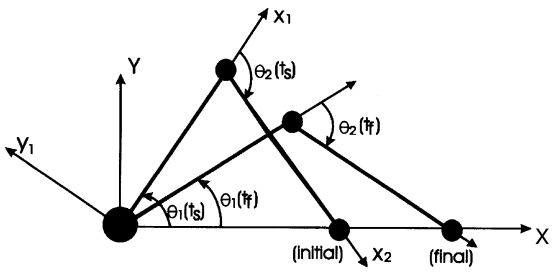

Fig. 6. Initial and final states of a planar elbow arm.

Table IV. Link parameters of a planar elbow arm.

Link	J_h [kg.m^2]	M_t [kg]	l [m]	ρ [kg/m]	EI [N.m^2]
Upperarm	0.1042	6.14	0.60	0.5033	1050
Forearm	0.1042	0	0.55	0.5033	1050

Let $r_d(t)$ denote the reference endpoint trajectory with respect to the inertia frame, then the reference trajectories of the link tips are obtained by solving the inverse kinematics problem:

$$\boldsymbol{y}_d(t) = \begin{bmatrix} \arccos\left(\dfrac{l_1^2 - l_2^2 + r_d^2}{2 l_1 r_d}\right) \\ \arccos\left(\dfrac{l_1^2 + l_2^2 - r_d^2}{2 l_1 l_2} - \pi\right) \end{bmatrix}.$$

Here we assume that $\theta_1 \le \theta_2$ for the elbow-up configuration. The endpoint reference trajectory and the link tip trajectories are plotted in Figure 7. Figure 8 shows the calculated torque trajectories, generated by the perturbed inverse dynamics developed here, which are compared with those obtained by the rigid inverse dynamics when ignoring link flexibility. Two assumed modes are used to model the planar elbow arm. The inverse dynamics control design for tracking the above endpoint reference trajectory has been simulated using $\boldsymbol{K}_{p0} = \boldsymbol{K}_{d0} = \mathbf{diag(18.6, 6.0)}$. The additional torque trajectories for stabilizing the error dynamics are shown in Figure 9, and the tracking error profiles of the link tips are compared with those without stabilizing the error dynamics in Figure 10. In short, these numerical results show that incorporating with feedback stabilizing control, the feedforward commands generated by the new formulation of the inverse dynamics can achieve asymptotically exact tracking of the reference endpoint trajectory.

https://doi.org/10.1017/S0263574701003526 Published online by Cambridge University Press

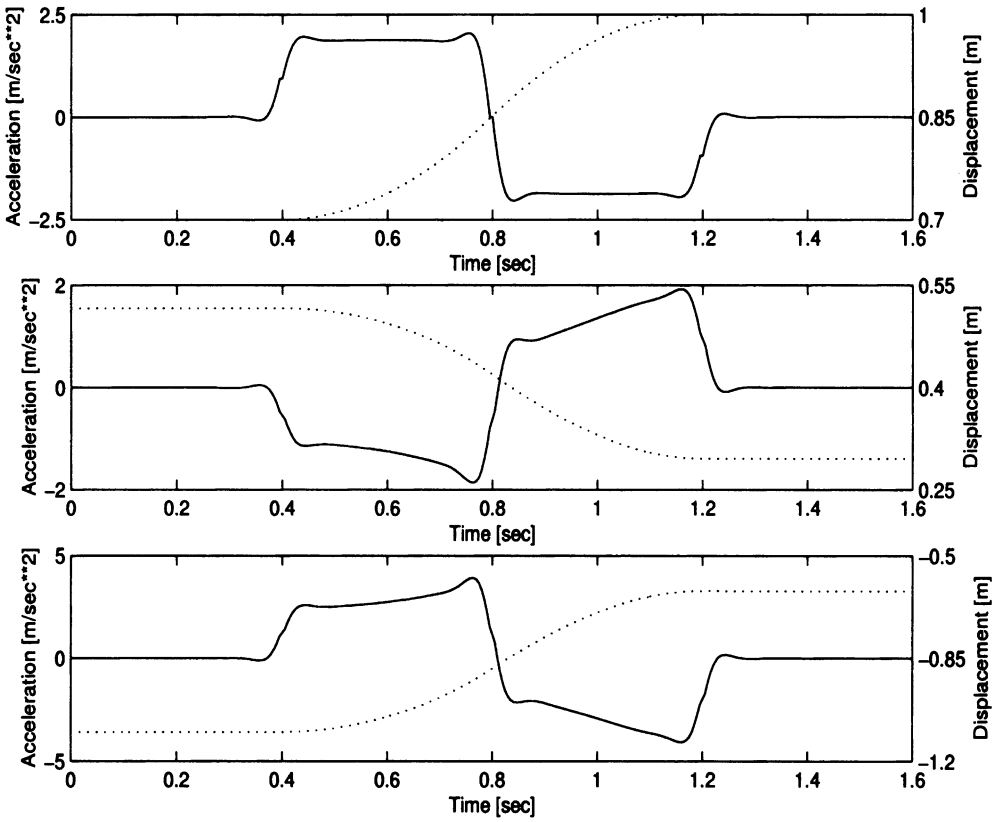

Fig. 7. Reference trajectories: (top) arm endpoint; (middle) upperarm tip (bottom) forearm tip; solid line for acceleration; dotted line for displacement.

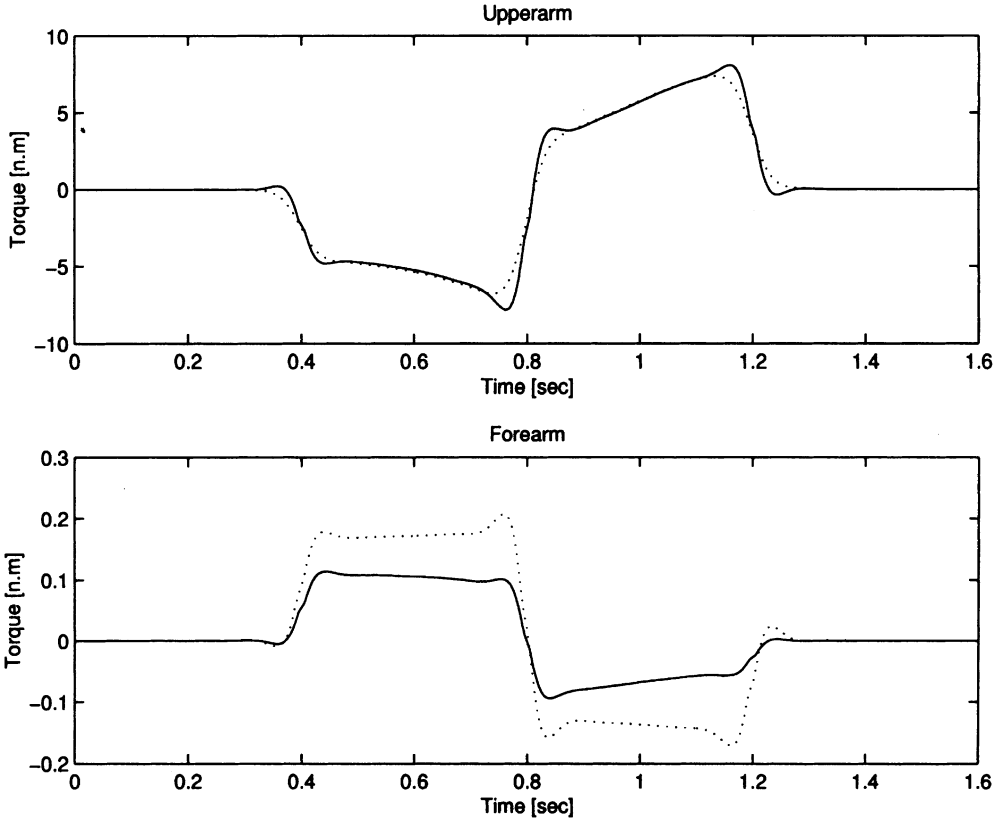

Fig. 8. Calculated torque trajectories: (top) upperarm; (bottom) forearm; solid line for the rigid dynamics; dotted line for the new formulation.

https://doi.org/10.1017/S0263574701003526 Published online by Cambridge University Press

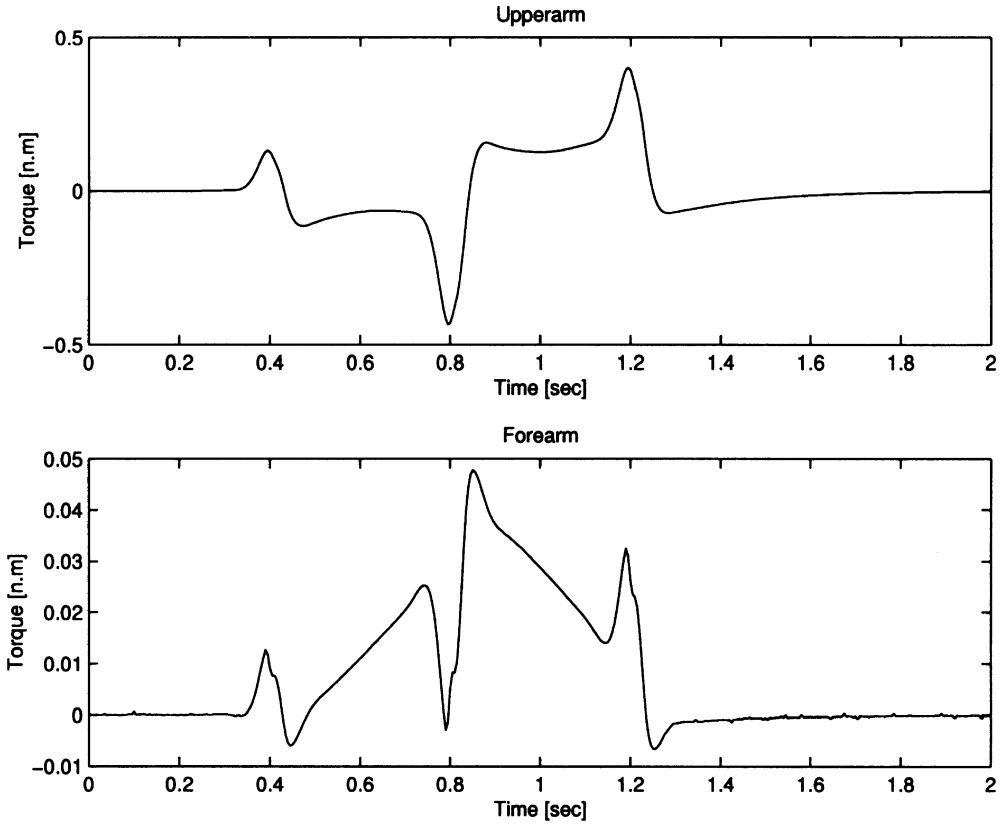

Fig. 9. Additional torque trajectories: (top) upperarm; (bottom) forearm.

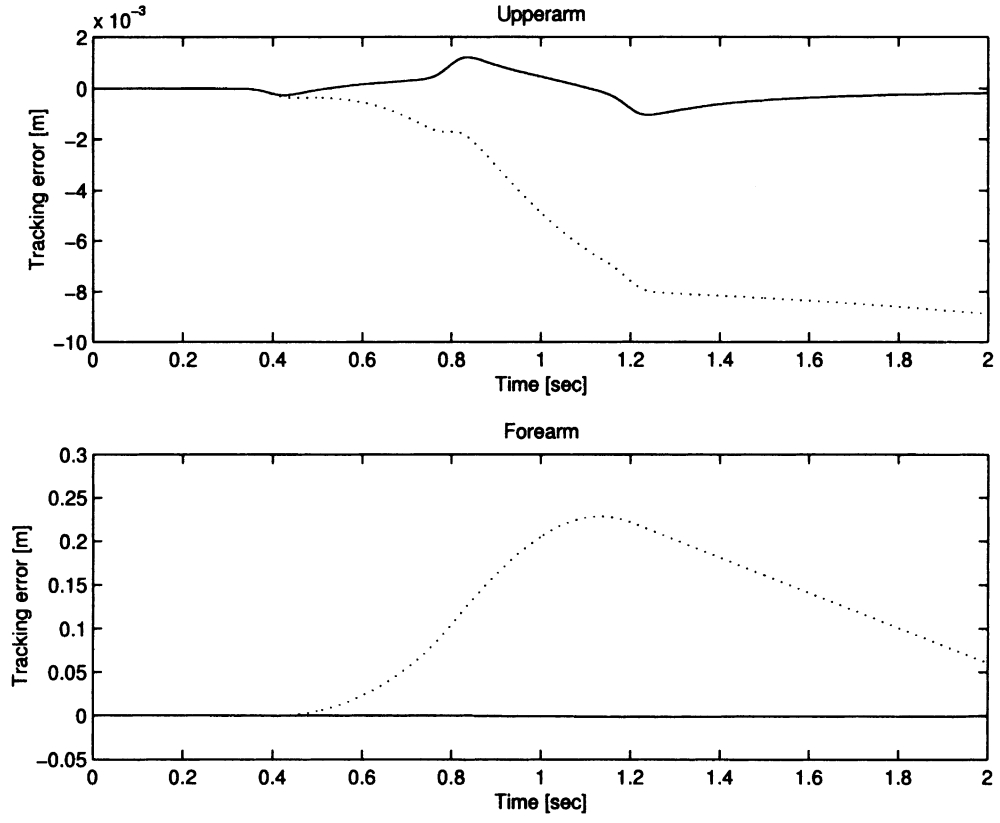

Fig. 10. Tracking errors: (top) upperarm; (bottom) forearm; solid line for the case with feedback stabilizing; dotted line for the case without feedback stabilizing.

https://doi.org/10.1017/S0263574701003526 Published online by Cambridge University Press

CONCLUSIONS

There are two main contributions of this paper: (i) The jumping behavior of the ill-defined relative degree of a flexible manipulator is revealed by constructing a perturbed truncation model; (ii) Based on the perturbed truncation model in the extreme case, that is, truncating all transients of the flexible dynamics, the inverse dynamics control design is reformulated in a novel way.

The departual point of this work is the multi-time-scale characteristics of the dynamics of a flexible manipulator. This allows us to treat the flexible dynamics as fast-time-scale perturbations to the rigid dynamics. To account for the contributions from the flexible dynamics in constructing the finite dimensional approximation, we retain all quasi-steady-states of the flexible dynamics as perturbations but truncate their transients. In this way, the perturbed truncation model is much more attractive than that obtained by the direct truncation. The first important thing for this perturbed truncation model is that it can predict the jumping behavior of the ill-defined relative degree which the direct truncation cannot offer. This is a new consideration on this aspect. In addition, the inverse dynamics control design can benefit from the perturbed truncation. With the perturbed truncation, the inverse dynamics control design can be used to track trajectories being unnecessarily differentiable, thus it holds great promise for a much wider range of practical applications. Also, the perturbed truncation leads to nearly linear and time-invariant internal dynamics with a relatively lower order for a multi-link flexible manipulator. Its simplicity makes the inverse dynamics control design practically useful.

ACKNOWLEDGEMENT

The first author acknowledges the support of the Alexander von Humboldt Foundation of Germany.

APPENDIX A

Neglecting the effect of the shear deformation and rotatory inertia, and according to Euler-Bernoulli beam theory, the motion equations of a planar single-link flexible manipulator are

$$\rho\ddot{z}(t, x)+EI\mathrm{D}^4z(t, x)=0,\ t\geq 0,\ 0\leq x\leq l, \tag{45}$$

$$J_h\ddot{\theta}(t)-EI\mathrm{D}^2z(t, 0)=\tau(t),\ t\geq 0, \tag{46}$$

with the boundary conditions

$$z(t, 0)=0,\ \mathrm{D}z(t, 0)=\theta(t), \tag{47}$$

$$M_t\ddot{z}(t, l)=EI\mathrm{D}^3z(t, l),\ EI\mathrm{D}^2z(t, l)=0. \tag{48}$$

The differential notations used here are $\mathrm{D}f=\partial f/\partial x$ and $\dot{f}=\partial f/\partial t$. The modal expansion of $z(t, x)$ is $z(t, x)=\sum_{n=0}^{\infty}\phi_n(x)q_n(t)$, where $q_n(t)$ is the modal coordinate of the nth unconstrained mode function $\phi_n(x)$. It is convenient to write it in dimensionless form by defining

$$\chi=x/l,\ \bar{\phi}_n(\chi)=\phi_n(x)/l,\ \mathrm{D}^i\bar{\phi}_n(\chi)=l^{i-1}\mathrm{D}^i\phi_n(x).$$

For periodical solutions $q_n(t)=e^{j\omega_n t}$, where ω_n is the natural frequency of the nth mode. Inserting the modal expansion in dimensionless form into (45)–(48) gives

$$\mathrm{D}^4\bar{\phi}_n=d_n^4\bar{\phi}_n,$$

where $d_n^4=\rho l^4\omega_n^2/EI$ and the boundary conditions

$$\bar{\phi}_n(0)=0,\ \frac{J_h d_n^4}{\rho l^3}D\bar{\phi}_n(0)+D^2\bar{\phi}_n(0)=0,$$

$$D^3\bar{\phi}_n(1)=-\frac{M_t d_n^4}{l\rho}\bar{\phi}_n(1),\ EID^2\bar{\phi}_n(1)=0.$$

The general solution for $\bar{\phi}_n$ can be expressed by

$$\bar{\phi}_n(\chi)=F_{1,n}\sin d_n\chi+F_{2,n}\sinh d_n\chi+F_{3,n}\cos d_n\chi+F_{4,n}\cosh d_n\chi.$$

The above boundary conditions are more conveniently expressed in matrix form

$$[n_{ij}(d_n)]\begin{bmatrix}F_{1,n}\\F_{2,n}\\F_{3,n}\end{bmatrix}=\begin{bmatrix}0\\0\\0\end{bmatrix},$$

where n_{ij} are given by

$$n_{11}(d_n)=-\cos d_n+\frac{M_t d_n}{l\rho}\sin d_n,$$

$$n_{12}(d_n)=\cosh d_n+\frac{M_t d_n}{l\rho}\sinh d_n,$$

$$n_{13}(d_n)=\sin d_n-\sinh d_n+\frac{M_t d_n}{l\rho}(\cos d_n-\cosh d_n),$$

$$n_{21}(d_n)=-\sin d_n,$$

$$n_{22}(d_n)=\sinh d_n,$$

$$n_{23}(d_n)=-\cos d_n-\cosh d_n,$$

$$n_{31}(d_n)=-\frac{J_h d_n^5}{l^3\rho},$$

$$n_{32}(d_n)=-\frac{J_h d_n^5}{l^3\rho},$$

$$n_{33}(d_n)=2d_n^2.$$

For non-trivial solutions, $\det([n_{ij}(d_n)])=0$, giving the characteristic equation:

$$Q(d_n):=(\sin d_n\cosh d_n-\cos d_n\sinh d_n)+\frac{J_h d_n^3}{\rho l^3}(1+\cos d_n\cosh d_n)+2\frac{M_t d_n}{\rho l}\sin d_n\sinh d_n+\frac{J_h M_t d_n^4}{\rho l^4}(\cos d_n\sinh d_n-\sin d_n\cosh d_n)=0.$$

For larger number n, we have

$$(d_n^{-4}e^{-d_n})Q(d_n)\approx\frac{J_h M_t}{\rho l^4}(\cos d_n-\sin d_n),$$

https://doi.org/10.1017/S0263574701003526 Published online by Cambridge University Press

which implies that d_n tends to satisfy $\cos d_n - \sin d_n = 0$, thus d_n has the asymptotic expression as

$$d_n \approx \left(n+\frac{1}{4}\right)\pi,$$

that is, $\omega_n^2 = O(n^4)$. Here $O(h)$ denotes a term of order h, i.e., $|O(h)| < kh$ for some fixed $k>0$. For each n, the constants $F_{2,n}$ and $F_{3,n}$ can be expressed in terms of $F_{1,n}$ and d_n. To fix $F_{1,n}$, use is made of the orthogonality properties of the modes

$$\int_0^l \rho\phi_i(x)\phi_j(x)\,\mathrm{d}x + M_t\varphi_i\varphi_j + J_h\psi_i\psi_j = \delta_{ij},$$

where δ_{ij} is the Kronecker delta. Multiply (45) by $\phi_n(x)$ and integrate it from 0 to l, applying the above orthogonality property yields the modal equation in the form of

$$\ddot{q}_n + \omega_n^2 q_n = \psi_n \tau.$$

For larger number n, it is easily verified that φ_n and ψ_n tend to be

$$\varphi_n \approx (-1)^n\sqrt{2}l(F_{1,n} - F_{2,n}),$$

$$\psi_n \approx \frac{\rho l^3}{J_h}\left(n+\frac{1}{4}\right)^{-2}\pi^{-2}F_{3,n},$$

and $F_{i,n}$, $i=1, 2, 3$, tend to be

$$F_{1,n} \approx F_{3,n} \approx -F_{2,n} \approx F = (8M_t l^2 + \rho l^3)^{-1/2}.$$

These together imply the following asymptotic expressions

$$\varphi_n\psi_n \approx (-1)^n 2\sqrt{2}\,\frac{\rho l^4}{J_h}\left(n+\frac{1}{4}\right)^{-2}\pi^{-2}F^2.$$

It is straightforward to verify that $\{[\phi_n(x)\ \varphi_n\ \psi_n]^T\}$ forms a complete orthonormal system in $L^2(0, l)\times\mathbb{R}^2$ endowed with the inner products

$$\langle u, v\rangle = \int_0^l \rho u_1 v_1 dx + M_t u_2 v_2 + J_h u_3 v_3.$$

We expand $[0\ 0\ J_h]^T$ in $L^2(0,l)\times\mathbb{R}^2$ as

$$\begin{bmatrix} 0 \\ 0 \\ J_h \end{bmatrix} = \sum_{n=0}^{\infty} \psi_n \begin{bmatrix} \phi_n(x) \\ \varphi_n \\ \psi_n \end{bmatrix},$$

in which the second component is

$$\sum_n^{\infty} \varphi_n\psi_n = 0.$$

Let $\tilde{\epsilon}_N = \sum_{n=0}^{N} \varphi_n\psi_n = -\sum_{n=N+1}^{\infty} \varphi_n\psi_n$. Note that $(-1)^n\varphi_n\psi_n > 0$ decreases strictly as n increases, thus we have

$$\tilde{\epsilon}_N = (-1)^N |O(\varphi_{N+1}\psi_{N+1})| = (-1)^N |O((N+1)^{-2})|.$$

Also, for the term $\bar{\epsilon}_N = \sum_{n=N+1}^{\infty} \omega_n^{-2}\varphi_n\psi_n$, note that $(-1)^n\omega_n^{-2}\varphi_n\psi_n > 0$ decreases strictly as n increases, thus we have

$$\bar{\epsilon}_N = (-1)^{N+1} |O(\omega_{N+1}^{-2}\varphi_{N+1}\psi_{N+1})| = (-1)^{N+1} |O((N+1)^{-6})|.$$

APPENDIX B

Hereafter, we use the notations $\bar{\lambda}(\cdot)$ and $\underline{\lambda}(\cdot)$ to indicate the largest and smallest eigenvalues of a matrix, respectively. The Euclidean norm for a vector is used, that is, $\|\boldsymbol{q}\| = \sqrt{\boldsymbol{q}^T\boldsymbol{q}}$. The norm of a matrix $\boldsymbol{H}$ is corresponding induced norm $\|\boldsymbol{H}\| = \sqrt{\bar{\lambda}(\boldsymbol{H}^T\boldsymbol{H})}$. Some well-known properties of the dynamic model (22) under the small deformation assumption, which are used in the sequel, are summarized as follows

(P1) $\boldsymbol{H}(\boldsymbol{q})$ is symmetric positive definite and there exists $k_m > 0$ such that for any $\boldsymbol{q}, \bar{\boldsymbol{q}} \in \mathbb{R}^{N_f}$

$$\|\boldsymbol{H}(\boldsymbol{q}) - \boldsymbol{H}(\bar{\boldsymbol{q}})\| \le \|\boldsymbol{q} - \bar{\boldsymbol{q}}\|;$$

(P2) there exist $k_{c1} > 0$ and $k_{c2} > 0$ such that for any $\boldsymbol{q}, \bar{\boldsymbol{q}} \in \mathbb{R}^{N_f}$

$$\|\boldsymbol{C}(\boldsymbol{q},\dot{\boldsymbol{q}}) - \boldsymbol{C}(\bar{\boldsymbol{q}},\dot{\bar{\boldsymbol{q}}})\| \le k_{c1}\|\dot{\boldsymbol{q}} - \dot{\bar{\boldsymbol{q}}}\| + k_{c2}\|\dot{\bar{\boldsymbol{q}}}\|\|\boldsymbol{q} - \bar{\boldsymbol{q}}\|,$$

and

$$\|\boldsymbol{C}(\boldsymbol{q}, \dot{\boldsymbol{q}})\| \le k_{c1}\|\dot{\boldsymbol{q}}\|;$$

(P3) the matrix $\dot{\boldsymbol{H}}(\boldsymbol{q}) - 2\boldsymbol{C}(\boldsymbol{q}, \dot{\boldsymbol{q}})$ is skew symmetric, that is,

$$\dot{\boldsymbol{H}}(\boldsymbol{q}) = \boldsymbol{C}(\boldsymbol{q},\dot{\boldsymbol{q}}) + \boldsymbol{C}(\boldsymbol{q},\dot{\boldsymbol{q}})^T;$$

(P4) the matrices $\boldsymbol{K}$ and $\boldsymbol{D}$ are diagonal and positive definite.

Note the quasi-steady-states of the fast modes are constant during fast transient, that is, $\dot{\bar{\boldsymbol{q}}}_f = \ddot{\bar{\boldsymbol{q}}}_f = \boldsymbol{0}$. Let $\boldsymbol{\tau}_e$ denote the additional torque that is used to stabilize the error dynamics. Applying $\boldsymbol{\tau} = \bar{\boldsymbol{\tau}}_d + \boldsymbol{\tau}_e$ to (22) yields the error dynamics of

$$\boldsymbol{H}(\boldsymbol{q})\ddot{\boldsymbol{e}} + \boldsymbol{K}_e\boldsymbol{e} + \boldsymbol{D}_e\dot{\boldsymbol{e}} + (\boldsymbol{H}(\boldsymbol{q}) - \boldsymbol{H}(\bar{\boldsymbol{q}}_0))\ddot{\bar{\boldsymbol{q}}} + \boldsymbol{H}_c(\boldsymbol{q}, \dot{\boldsymbol{q}}) - \boldsymbol{H}_c(\bar{\boldsymbol{q}}_0, \dot{\bar{\boldsymbol{q}}}_0) = \boldsymbol{B}\boldsymbol{\tau}_e, \tag{49}$$

where $\boldsymbol{e} = \boldsymbol{q} - \bar{\boldsymbol{q}}$ or $[\boldsymbol{e}_0^T\ \boldsymbol{e}_f^T]^T = [\boldsymbol{q}_0^T - \bar{\boldsymbol{q}}_0^T\ \boldsymbol{q}_f^T - \bar{\boldsymbol{q}}_f^T]^T$. The resulting tracking error is

$$\boldsymbol{y}_e = \boldsymbol{\Phi}_0\boldsymbol{e}_0 + \boldsymbol{\Phi}_f^T\boldsymbol{e}_f. \tag{50}$$

Consider the Lyapunov candidate function given by

$$V = \frac{1}{2}\begin{bmatrix} \boldsymbol{e} \\ \dot{\boldsymbol{e}} \end{bmatrix}^T \begin{bmatrix} \boldsymbol{K}_p + \upsilon\boldsymbol{K}_d & \upsilon\boldsymbol{H}(\boldsymbol{q}) \\ \upsilon\boldsymbol{H}(\boldsymbol{q}) & \boldsymbol{H}(\boldsymbol{q}) \end{bmatrix} \begin{bmatrix} \boldsymbol{e} \\ \dot{\boldsymbol{e}} \end{bmatrix}, \tag{51}$$

where $\upsilon > 0$ is a scalar, $\boldsymbol{K}_p = \mathrm{diagblock}(\boldsymbol{K}_{p0}, \boldsymbol{K})$ and $\boldsymbol{K}_d = \mathrm{diagblock}(\boldsymbol{K}_{d0}, \boldsymbol{D})$. Here $N\times N$ matrices $\boldsymbol{K}_{p0}$ and $\boldsymbol{K}_{d0}$ are diagonal and positive definite. V is a positive definite function if and only if[34]

$$\boldsymbol{K}_p + \upsilon\boldsymbol{K}_d > \upsilon^2\boldsymbol{H}(\boldsymbol{q}). \tag{52}$$

https://doi.org/10.1017/S0263574701003526 Published online by Cambridge University Press

Differentiating this function with respect to time yields

$$\dot{V}=\boldsymbol{e}^T(\boldsymbol{K}_p+\upsilon\boldsymbol{K}_d)\dot{\boldsymbol{e}}+\upsilon\dot{\boldsymbol{e}}^T\boldsymbol{H}(\boldsymbol{q})\dot{\boldsymbol{e}}+\frac{1}{2}\upsilon\dot{\boldsymbol{e}}^T\dot{\boldsymbol{H}}(\boldsymbol{q})\boldsymbol{e}+$$

$$(\upsilon\boldsymbol{e}+\dot{\boldsymbol{e}})^T\left(\boldsymbol{H}(\boldsymbol{q})\ddot{\boldsymbol{e}}+\frac{1}{2}\dot{\boldsymbol{H}}(\boldsymbol{q})\dot{\boldsymbol{e}}\right). \tag{53}$$

Solving for $\boldsymbol{H}(\boldsymbol{q})\ddot{\boldsymbol{e}}$ in (49) and substituting it into (53) with the property (P3) gives

$$\dot{V}=\dot{\boldsymbol{e}}^T(\boldsymbol{K}_p+\upsilon\boldsymbol{K}_d)\dot{\boldsymbol{e}}+\upsilon\dot{\boldsymbol{e}}^T\boldsymbol{H}(\boldsymbol{q})\dot{\boldsymbol{q}}+\upsilon\dot{\boldsymbol{e}}^T\boldsymbol{C}(\boldsymbol{q},\dot{\boldsymbol{q}})\boldsymbol{e}+$$
$$(\upsilon\boldsymbol{e}+\dot{\boldsymbol{e}})^T(\boldsymbol{B}\boldsymbol{\tau}_e-\boldsymbol{K}_e\boldsymbol{e}-\boldsymbol{D}_e\dot{\boldsymbol{e}}+\boldsymbol{\lambda}), \tag{54}$$

where $\boldsymbol{\lambda}$ is given by

$$\boldsymbol{\lambda}=(\boldsymbol{H}(\bar{\boldsymbol{q}}_0)-\boldsymbol{H}(\boldsymbol{q}))\ddot{\bar{\boldsymbol{q}}}+(\boldsymbol{C}(\bar{\boldsymbol{q}}_0,\dot{\bar{\boldsymbol{q}}}_0)-\boldsymbol{C}(\boldsymbol{q},\dot{\boldsymbol{q}}))\dot{\bar{\boldsymbol{q}}}.$$

Recalling the properties (P1) and (P2) we have the estimation as

$$\begin{aligned}\|\boldsymbol{\lambda}\| &\le (\|\boldsymbol{H}(\bar{\boldsymbol{q}}_0)-\boldsymbol{H}(\boldsymbol{q})\|)\|\ddot{\bar{\boldsymbol{q}}}_0\|+\|\boldsymbol{C}(\bar{\boldsymbol{q}}_0,\dot{\bar{\boldsymbol{q}}}_0)-\boldsymbol{C}(\bar{\boldsymbol{q}},\dot{\bar{\boldsymbol{q}}}_0)\|\,\|\dot{\bar{\boldsymbol{q}}}_0\|\\ &\le (k_m\|\ddot{\bar{\boldsymbol{q}}}_0\|+k_{c2}\|\dot{\bar{\boldsymbol{q}}}_0\|^2)\|\boldsymbol{e}\|+k_{c1}\|\dot{\bar{\boldsymbol{q}}}_0\|\,\|\dot{\boldsymbol{e}}\|\\ &=:c_1(\ddot{\bar{\boldsymbol{q}}}_0,\dot{\bar{\boldsymbol{q}}}_0)\|\boldsymbol{e}\|+c_2(\dot{\bar{\boldsymbol{q}}}_0)\|\dot{\boldsymbol{e}}\|.\end{aligned}$$

With this in mind, we take the feedback control law as the form of

$$\boldsymbol{\tau}_e=-\boldsymbol{K}_{p0}\boldsymbol{e}_0-\boldsymbol{K}_{d0}\dot{\boldsymbol{e}}_0, \tag{55}$$

then (54) becomes

$$\begin{aligned}\dot{V} &\le \upsilon\dot{\boldsymbol{e}}^T\boldsymbol{H}(\boldsymbol{q})\dot{\boldsymbol{e}}-\dot{\boldsymbol{e}}^T\boldsymbol{K}_d\dot{\boldsymbol{e}}-\upsilon\boldsymbol{e}^T\boldsymbol{K}_p\boldsymbol{e}+\upsilon c_1\|\boldsymbol{e}\|^2\\ &\quad+(c_1+\upsilon c_2)\|\boldsymbol{e}\|\,\|\dot{\boldsymbol{e}}\|+c_2\|\dot{\boldsymbol{e}}\|^2+\upsilon k_{c1}\|\boldsymbol{e}\|\,\|\dot{\boldsymbol{e}}\|^2 \qquad (56)\\ &\le -\begin{bmatrix}\|\boldsymbol{e}\|\\ \|\dot{\boldsymbol{e}}\|\end{bmatrix}^T\Lambda\begin{bmatrix}\|\boldsymbol{e}\|\\ \|\dot{\boldsymbol{e}}\|\end{bmatrix}+\upsilon k_{c1}\|\boldsymbol{e}\|\,\|\dot{\boldsymbol{e}}\|^2,\end{aligned}$$

where

$$\Lambda=\begin{bmatrix}\upsilon(\underline{\lambda}(\boldsymbol{K}_p)-c_1) & -(c_1+\upsilon c_2)/2\\ -(c_1+\upsilon c_2)/2 & \underline{\lambda}(\boldsymbol{K}_d)-\upsilon\bar{\lambda}(\boldsymbol{H})-c_2\end{bmatrix}.$$

For smaller values of $\|\boldsymbol{e}\|$ and $\|\dot{\boldsymbol{e}}\|$, the quadratic term in the left hand side of (56) dominates the cubic one. Therefore, if Λ is positive definite, then $\dot{V}$ will be a locally negative definite function. This is true if and only if[34]

$$\underline{\lambda}(\boldsymbol{K}_p)>c_1, \tag{57}$$

$$\underline{\lambda}(\boldsymbol{K}_d)>\frac{(c_1+\upsilon c_2)^2}{4\upsilon(\underline{\lambda}(\boldsymbol{K}_p)-c_1)}+\upsilon\bar{\lambda}(\boldsymbol{H})+c_2. \tag{58}$$

Also, (57) and (58) imply (52), thus they assure that V is positive definite. Note that $\ddot{\bar{\boldsymbol{q}}}_0$, $\dot{\bar{\boldsymbol{q}}}_0$ and $\bar{\boldsymbol{q}}_0$ are bounded solutions via solving the internal dynamics, thus c_1 and c_2 are bounded. Now we assume that the structure stiffness matrix $\boldsymbol{K}$ and the structure damping matrix $\boldsymbol{D}$ are in the form of

$$\boldsymbol{K}=\nu\boldsymbol{K}_s,\ \boldsymbol{D}=\nu\boldsymbol{D}_s,$$

where $\nu>0$ is a structure design parameter. This means that the structure stiffness and damping can provide passive control. With this assumption, selecting appropriate $\upsilon>0$, $\nu>0$, $\boldsymbol{K}_{p0}$ and $\boldsymbol{K}_{d0}$ in agreement with (57) and (58) can assure that V is a positive definite function and $\dot{V}$ a negative definite function. This means that $\boldsymbol{e}(t)\to\boldsymbol{0}$, thus $\boldsymbol{y}_e(t)\to\boldsymbol{0}$, as $t\to\infty$. In short, the joint-based PD type feedback control law in (55) integrated with the structure passive control can be used to stabilize the error dynamics locally.

References

1. J. Chen, L Qiu and O. Toker, "Limitations on maximal tracking accuracy", *IEEE Transaction on Automatic Control* **45**, 326–331 (2000).
2. E. Bayo, P. Papadopoulos, J.Stubbe and M.A. Serna, "Inverse dynamics and kinematics of multi-link elastic robots: an iterative frequency domain approach", *Int. J. Robotics Research* **8**, 49–62 (1989).
3. D.-S. Kwon and W.J. Book, "A time-domain inverse dynamic tracking control of a single-link manipulator", *ASME Journal of Dynamics, Systems, Measurement, and Control* **116**, 193–200 (1994).
4. B. Paden, D. Chen, R. Ledesma and E. Bayo, "Exponentially stable tracking control for multi-joint flexible-link manipulators", *ASME Journal Dynamics Systems, Measurement, and Control* **115**, 53–59 (1993).
5. A. De Luca, S. Panzieri and G. Ulivi, "Stable inversion control for flexible link manipulators", *Proceedings of IEEE Conference on Robotics and Automation* (Inst. of Electrical and Electronics Engineers, 1998) pp 799–805.
6. S. Devasia, D. Chen and B. Paden, "Nonlinear inversion-base output tracking", *IEEE Trans. Automatic Control* **41**, 930–942 (1996).
7. D. Chen and B. Paden, "Stable inversion of nonlinear non minimum phase systems", *Int. J. Control* **64**, 81–97 (1996).
8. L.R. Hunt, G. Meyer and R.J. Su, "Noncausal inverse for linear systems", *IEEE Transaction on Antomatic Control* **41**, 608–611 (1996).
9. L.R. Hunt and G. Meyer, "Stable inversion for nonlinear systems", *Automatica* **33**, 1549–1554 (1997).
10. G. Meyer, L.R. Hunt and R. Su, "Nonlinear system guidance in the presence of transmission zero dynamics", *Technical Report Tech. Memo. 4661* (NASA, 1995).
11. P. Martin, S. Devasia and B. Paden, "A different look at output tracking: control of a VTOL aircraft", *Automatica* **32**, 101–107 (1996).
12. A. Isidori and C.I. Byrnes, "Output regulation of nonlinear systems", *IEEE Transaction on Automatic Control* **35**, 131–140 (1990).
13. R.M. Hirschorn, "Invertibility of multivariable nonlinear control system", *IEEE Transaction on Automatic Control* **24**, 855–865 (1979).
14. M.D. Di Benedetto and P. Lucibello, "Inversion of nonlinear time-varying systems", *IEEE Transaction on Automatic Control* **38**, 1259–1264 (1993).
15. D. Wang and M. Vidyasagar, "Control of a class of manipulators with a single flexible link – part 1: feedback linearization", *ASME Journal Dynamics Systems, Measurement, and Control* **113**, 655–661 (1991).
16. D. Wang and M. Vidyasagar, "Transfer functions for a single-link flexible link", *Int. J. Robotics Research* **10**, 540–549 (1992).
17. G. Wang and G. Lu, "Well-posedness of inverse dynamics of flexible robot arms", *Int. J. Robotics and Automation* **4**, 175–182 (1996).
18. E. Bayo and B. Paden, "On trajectory generation for flexible robots", *J. Robotic Systems* **4**, 229–235 (1987).
19. H. C. Moulin and E. Bayo, "Acceleration profiles for causal solutions of the inverse dynamics approach to the control of single link flexible arms", *ASME Journal Dynamics Systems, Measurement, and Control* **113**, 752–754 (1991).

https://doi.org/10.1017/S0263574701003526 Published online by Cambridge University Press

20. M.A. Serna and E. Bayo, "Trajectory planning for flexible manipulators", *Proceedings of IEEE Conference on Robotics and Automation* (Inst. of Electrical and Electronics Engineers, 1990) pp. 910–915.
21. N Fabritz, *Ein offenes Automatisierungssystem für einen mehrgliedrigen elastischen Manipulator* (VDI Verlag, Dusseldorf, 1997).
22. E. Barbieri, "Single-input/single-output transfer functions for a flexible slewing link", *J. Robotics Systems* **10**, 325–344 (1993).
23. A. De Luca, P. Lucibello and G. Ulivi, "Inversion techniques for trajectory control of flexible robot arms", *J. Robotic Systems* **6**, 325–344 (1989).
24. A. De Luca and B. Siciliano, "Inversion-based nonlinear control of robot arms with flexible links", *AIAA Journal of Guidance, Control and Dynamics* **16**, 1169–1176 (1993).
25. C.J. Damaren, "Approximate inverse dynamics and passive feedback for flexible manipulator with large payloads", *IEEE Transaction on Robotics and Automation* **12**, 131–138 (1996).
26. A.R. Fraser and R.W. Daniel, *Perturbation Techniques for Flexible Manipulators* (Kluwer Academic Publisher, New York, 1991).
27. P.V. Kokotović, H.A. Khalil and J.O'Reilly, *Singular Perturbation Methods in Control: Analysis and Design* (Academic Press, London, 1986).
28. B. Siciliano and W.J. Book, "A singular perturbation approach to control of light-weight flexible manipulators", *Int. J. Robotics Research* **7**, 79–90 (1988).
29. M.W. Vandegrift, F.L. Lewis and S. Zhu, "Flexible-link robot arm control by a feedback linearization/singular perturbation approach", *J. Robotics Systems* **10**, 591–603 (1994).
30. E. Bayo, R. Movaghar and M. Medus, "Inverse dynamics of a single-link flexible robot: analytical and experimental results", *Int. J. Robotics and Automation* **3**, 150–156 (1988).
31. C.J. Tomlin and S.S. Sastry, "Bounded tracking for non-minimum phase nonlinear systems with fast zero dynamics", *Int. J. Control* **68**, 819–847 (1997).
32. J. Hauser, S. Sastry and G. Meyer, "Nonlinear control design for slightly nonminimum phase system: application to V/CTOL aircraft", *Automatica* **28**, 665–679 (1992).
33. A. Preumont, *Vibration Control of Active Structure* (Kluwer Academic Publishers, Dordrecht, 1997).
34. R.E. Skelton, T. Iwasaki and K. Grigoriadis, *A Unified Algebraic Approach to Linear Control Design* (Taylor & Francis, London, 1998).

https://doi.org/10.1017/S0263574701003526 Published online by Cambridge University Press